

Pan-STARRS and PESSTO search for an optical counterpart to the LIGO gravitational wave source GW150914

S. J. Smartt^{1*}, K. C. Chambers², K. W. Smith¹, M. E. Huber², D. R. Young¹, E. Cappellaro¹⁵, D. E. Wright¹, M. Coughlin³, A. S. B. Schultz², L. Denneau², H. Flewelling², A. Heinze², E. A. Magnier², N. Primak², A. Rest⁴, A. Sherstyuk², B. Stalder², C. W. Stubbs³, J. Tonry², C. Waters², M. Willman², J. P. Anderson¹⁰, C. Baltay²⁴, M. T. Botticella¹⁹, H. Campbell¹⁶, M. Dennefeld⁵, T.-W. Chen⁹, M. Della Valle¹⁹, N. Elias-Rosa¹⁵, M. Fraser¹⁶, C. Inserra¹, E. Kankare¹, R. Kotak¹, T. Kupfer^{20,24}, J. Harmanen¹⁴, L. Galbany^{12,13}, A. Gal-Yam²⁶, L. Le Guillou^{6,7}, J. D. Lyman⁸, K. Maguire¹, A. Mitra⁷, M. Nicholl¹¹, F. Olivares E^{12,23}, D. Rabinowitz²⁴, A. Razza^{12,13}, J. Sollerman²¹, M. Smith²², G. Terreran^{15,1}, S. Valenti^{17,18}, B. Gibson², T. Goggia²

¹ *Astrophysics Research Centre, School of Mathematics and Physics, Queens University Belfast, Belfast BT7 1NN, UK*

² *Institute for Astronomy, University of Hawaii at Manoa, Honolulu, HI 96822, USA*

³ *Department of Physics, Harvard University, Cambridge, MA 02138, USA*

⁴ *Space Telescope Science Institute, 3700 San Martin Drive, Baltimore, MD 21218, USA*

⁵ *Institut d'Astrophysique de Paris, CNRS, and Universite Pierre et Marie Curie, 98 bis Boulevard Arago, 75014, Paris, France*

⁶ *Sorbonne Universites, UPMC Univ. Paris 06, UMR 7585, LPNHE, F-75005, Paris, France*

⁷ *CNRS, UMR 7585, Laboratoire de Physique Nucleaire et des Hautes Energies, 4 place Jussieu, 75005 Paris, France*

⁸ *Department of Physics, University of Warwick, Coventry CV4 7AL, UK*

⁹ *Max-Planck-Institut für Extraterrestrische Physik, Giessenbachstraße 1, 85748, Garching, Germany*

¹⁰ *European Southern Observatory, Alonso de Cordova 3107, Vitacura, Santiago, Chile*

¹¹ *Harvard-Smithsonian Center for Astrophysics, 60 Garden St, Cambridge, MA 02138, United States*

¹² *Millennium Institute of Astrophysics, Casilla 36D, Santiago, Chile*

¹³ *Departamento de Astronomia, Universidad de Chile, Camino El Observatorio 1515, Las Condes, Santiago, Chile*

¹⁴ *Tuorla Observatory, Department of Physics and Astronomy, University of Turku, Väiäläntie 20, FI-21500 Piikkiö, Finland*

¹⁵ *INAF - Osservatorio Astronomico di Padova, Vicolo del l'Osservatorio 5, 35122 Padova, Italy*

¹⁶ *Institute of Astronomy, University of Cambridge, Madingley Road, Cambridge CB3 0HA, UK*

¹⁷ *Las Cumbres Observatory Global Telescope Network, 6740 Cortona Dr., Suite 102, Goleta, California 93117, USA*

¹⁸ *Department of Physics, University of California Santa Barbara, Santa Barbara, CA 93106, USA*

¹⁹ *INAF, Osservatorio Astronomico di Capodimonte, Salita Moiariello 16, 80131, Napoli, Italy*

²⁰ *California Institute of Technology, MC 290-17 Pasadena, CA, 91125, USA*

²¹ *Department of Astronomy and the Oskar Klein Centre, Stockholm University, AlbaNova, SE-106 91 Stockholm, Sweden*

²² *School of Physics and Astronomy, University of Southampton, Southampton, SO17 1BJ, UK*

²³ *Departamento de Ciencias Fisicas, Universidad Andres Bello, Avda. Republica 252, Santiago, Chile*

²⁴ *Division of Physics, Mathematics, and Astronomy, California Institute of Technology, Pasadena, CA 91125, USA*

²⁵ *Physics Department, Yale University, New Haven, CT 06520, USA*

²⁶ *Benozio Center for Astrophysics, Weizmann Institute of Science, 76100 Rehovot, Israel*

ABSTRACT

We searched for an optical counterpart to the first gravitational wave source discovered by LIGO (GW150914), using a combination of the Pan-STARRS1 wide-field telescope and the PESSTO spectroscopic follow-up programme. As the final LIGO sky maps changed during analysis, the total probability of the source being spatially coincident with our fields was finally only 4.2 per cent. Therefore we discuss our results primarily as a demonstration of the survey capability of Pan-STARRS and spectroscopic capability of PESSTO. We mapped out 442 square degrees of the northern sky region of the initial map. We discovered 56 astrophysical transients over a period of 41 days from the discovery of the source. Of these, 19 were spectroscopically classified and a further 13 have host galaxy redshifts. All transients appear to be fairly normal supernovae and AGN variability and none is obviously linked with GW150914. We illustrate the sensitivity of our survey by defining parameterised lightcurves with timescales of 4, 20 and 40 days and use the sensitivity of the Pan-STARRS1 images to set limits on the luminosities of possible sources. The Pan-STARRS1 images reach limiting magnitudes of $i_{P1} = 19.2, 20.0$ and 20.8 respectively for the three timescales. For long timescale parameterised lightcurves (with $\text{FWHM} \approx 40\text{d}$) we set upper limits of $M_i \leq -17.2_{+1.4}^{-0.9}$ if the distance to GW150914 is $D_L = 400 \pm 200$ Mpc. The number of type Ia SN we find in the survey is similar to that expected from the cosmic SN rate, indicating a reasonably complete efficiency in recovering supernova like transients out to $D_L = 400 \pm 200$ Mpc.

Key words: Gravitational waves – Supernovae: general – Gamma Ray Bursts: general

1 INTRODUCTION

The first observations of Advanced LIGO (aLIGO: The LIGO Scientific Collaboration et al. 2015), consisting of two 4 km gravitational-wave interferometers, one at Hanford, WA and the other at Livingston, LA began in September 2015 and ended January 2016. Advanced Virgo (Acernese et al. 2015) is due to come online in 2016. Due to significant instrumental upgrades (The LIGO Scientific Collaboration et al. 2015), the sensitivities in the LIGO interferometers have reached strain noise amplitudes below $10^{-23}\text{Hz}^{-1/2}$ in the frequency regime 10^2 to 10^3 Hz. The improved sensitivity over previous science runs (The LIGO Scientific Collaboration & The Virgo Collaboration 2012) is about a factor 3 in strain sensitivity in the most sensitive band, which corresponds to an increase in survey volume of more than an order of magnitude (see Abbott et al. 2016b).

Sources of gravitational-waves that the detectors are sensitive to are the compact binary coalescences of black holes and neutron stars and potentially asymmetric core-collapse of massive stars (Aasi et al. 2013; Abadie et al. 2012, 2010). The advanced gravitational-wave detectors are currently sensitive to binary neutron star mergers within about 100 Mpc (or beyond if black hole mergers are involved). The rate of such events is extremely uncertain, by several orders of magnitude, but the detectors are expected to be sensitive to a few neutron-star coalescences per year and potentially more for black hole mergers (Abadie et al. 2010). Compact binaries are one of the most promising sources for simultaneous detection of gravitational-wave and electromagnetic emission, which can occur on timescales from seconds to months and wavelengths from X-ray to radio (Metzger & Berger 2012; Metzger et al. 2010). One potential source of

electromagnetic emission from compact binaries containing at least one neutron star are kilonovae (Metzger et al. 2015; Tanvir et al. 2013; Berger, Fong & Chornock 2013). Compact binary mergers are the working model for short GRBs (with gamma-ray emission lasting less than ~ 2 sec) in which beamed high energy emission occurs due to observers being on the binary rotation axis (Narayan, Paczynski & Piran 1992). As discussed in Gehrels et al. (2015), short GRBs (sGRBs) have been observed from $0.2 \lesssim z \lesssim 2$ by *Swift* and indeed the kilonova candidate of Tanvir et al. (2013) was at $z = 0.356$. Another plausible candidate for a kilonova has been recently identified by Jin et al. (2015) and Yang et al. (2015) in the data for GRB060614 which likely has a host galaxy at $z = 0.125$. Gehrels et al. (2015) also point out that in 10.5 years of *Swift* operations, there have been no detections of sGRBs with redshifts $z < 0.1$. This corresponds to a distance of about 400 Mpc which is much further (a factor ~ 4) than the estimated sensitivity range of LIGO for NS-NS mergers. However the beaming factors for sGRBs is still quite uncertain and a much higher volumetric rate of NS-NS mergers is plausible if they are currently evading detection due to unfavourable beaming angles. Radiative transfer models of simulated NS-NS and BH-NS mergers predict a range of electromagnetic flux (e.g. Tanaka & Hotokezaka 2013; Barnes & Kasen 2013; Tanaka et al. 2014; Kasen, Fernández & Metzger 2015)

There are algorithms to localise the gravitational-wave transients on the sky, which vary from unmodeled sources (Essick et al. 2015; Cornish & Littenberg 2015) to compact binary signals (Singer et al. 2014; Berry et al. 2015; Chen & Holz 2015). These algorithms result in likelihood sky areas typically spanning $\approx 100 - 1000 \text{deg}^2$. The program we will discuss in this paper uses a sky-map produced by the unmodeled source algorithms. The initial LIGO and Virgo science runs included an electromagnetic

* Corresponding author Email : s.smartt@qub.ac.uk

follow-up program (Aasi et al. 2014), which has expanded for the recent run to include many partners. Efforts have been made to optimise the success of this program, including the use of gravitational-wave catalogs and optimising multiple-telescope pointings (White, Daw & Dhillon 2011; Kasliwal & Nissanke 2014; Nissanke, Kasliwal & Georgieva 2013; Gehrels et al. 2015; Cowperthwaite & Berger 2015; Berger 2014; Hanna, Mandel & Voutsden 2014), with lessons learned from other multi-messenger efforts (Aartsen et al. 2015; Singer et al. 2015; Cenko et al. 2013).

The first discovery of gravitational waves from a binary black Hole merger has been announced (Abbott et al. 2016b). The signal, known initially as candidate G184098, was initially announced on 16 September 2015 to the broad network of follow-up facilities who signed confidential Memoranda of Understanding with the LIGO/Virgo team. As discussed in Abbott et al. (2016b), the confirmed source GW150914 is a compact binary merger of two black holes with masses $M_1 = 36_{-4}^{+5} M_\odot$ and $M_2 = 29_{-4}^{+4} M_\odot$. GW150914 was found with a network signal to noise ratio of 24 corresponding to an $\approx 5.1\sigma$ detection. The distance to the source is estimated at $D = 410_{-180}^{+160}$ Mpc or $z = 0.09_{-0.04}^{+0.03}$, (see The LIGO Scientific Collaboration & the Virgo Collaboration 2016). From this event, Abbott et al. (2016b) and Abbott et al. (2016c) estimate the rate of BBH coalescences to be $0.002 - 0.4 \text{ Mpc}^{-3} \text{ Myr}^{-1}$ in the local Universe. To put this rate in perspective, we list the volumetric rates of various types of exploding transients in the Local Universe in Table 1. The rate of BBH mergers are surprisingly comparable other exotic transients we know of. The initial LIGO skymaps returned by the unmodeled pipelines returned sky-areas with 90% confidence levels of ≈ 310 square degrees, with the final LIGO analysis which was published corresponding to compact binary coalescences with skymaps covering 90% confidence levels of ≈ 600 square degrees. In this paper, we provide our first attempts to place upper-limits on optical counterparts to the direct detection of a gravitational wave signal.

This search for an optical counterpart to GW150914 requires pre-existing images of the available sky as well as the ability to survey the LIGO error regions efficiently. The Pan-STARRS facility and the Pan-STARRS1 Surveys (Chambers et al, 2016, in prep) provide the survey capability and the reference images. Analysis of the difference images by the Image Processing Pipeline or IPP (Wright et al. 2015) provides candidate detections and their attributes. These data are then further analysed by machine learning algorithms (Wright et al. 2015) to provide the down-selected list of candidates for follow-up spectroscopy by Hawaii and, the Public ESO Spectroscopic Survey of Transient Objects PESSTO. The Pan-STARRS1 telescope began its science surveys under the umbrella of the PS1 Science Consortium in 2010. These surveys ran until mid 2014, with the whole northern sky above a declination of $\delta \simeq -30^\circ$ degrees covered in the filters *grizy*_{P1} (called the 3π survey). The three other major surveys were the Medium Deep Field survey, as described in the papers Tonry et al. (2012a); Rest et al. (2014); McCrum et al. (2015), the Pandromeda project (Lee et al. 2014) and PanPlanets (Koppenhoefer et al. 2009). In addition an NEO focused survey on the sweet spots at opposition at the beginning and end of the nights was carried out (see Denneau et al. 2013, for a description of the PS1 moving

object processing system). The search for transients in the Medium Deep field has been well documented in, for example the recent papers of Chornock et al. (2014); Drout et al. (2014); Sanders et al. (2015); Gezari et al. (2015). A number of papers have used data from the 3π survey for transient science (e.g. Inserra et al. 2013b; Nicholl et al. 2013; Fraser et al. 2013). These have been a combination of finding and discovering transients in the 3π data (Polshaw et al. 2015; Inserra et al. 2013b) and retrospectively searching the data for interesting epochs for known supernovae and massive star outbursts (e.g. Fraser et al. 2013; Kankare et al. 2015).

Since the creation of an all-sky image stack (which was produced in a PS1 internal processing version called PV2) the single epochs in 3π have been differenced with respect to this reference sky and transients have been catalogued. The survey has transitioned from the PS1SC funded operations (2010 to mid-2014) to the Pan-STARRS Near Earth Object Science Consortium (PSNSC; mid-2014 to present) and the search for transients has continued. We currently run the ‘‘Pan-STARRS Survey for Transients’’ (PSST), with first results in Polshaw et al. (2015) and Huber et al. (2015a). We search the NASA PSNSC survey data for stationary transients and make our discoveries public on timescales of 12-24hrs after first observations. Additionally, we are using the Pan-STARRS1 telescope in pointed, triggered, mode to survey the sky localisation regions of LIGO/Virgo gravitational wave searches. This paper describes the first pointed search from this new operational mode of the PSNSC surveys. In doing this, we fed the targets discovered to two spectroscopic follow-up programmes. One of these was PESSTO, the Public ESO Spectroscopic Survey of Transient Objects which has 90 nights allocated per year on the ESO New Technology Telescope and has a partnership with Pan-STARRS to classify and follow targets from the PSST discovery stream (e.g. Le Guillou et al. 2015). The other was an extensive programme on the University of Hawaii 2.2m telescope with the SNIFS spectrometer.

2 INSTRUMENTATION AND OBSERVATIONAL DETAILS

2.1 The Pan-STARRS1 telescope, camera and photometric system

The Pan-STARRS1 telescope has a 1.8-m diameter primary mirror with $f/4.4$ cassegrain focus. It was designed as a high-étendue wide-field imaging system, and is located near the summit of Haleakala on the island of Maui. A 1.4 Gigapixel camera is mounted at cassegrain consisting of sixty Orthogonal Transfer Array devices, each of which has a detector area of 48460×48680 microns, of which 3.7 per cent is not active due to further division into OTA cells with gaps. The 10 micron pixels have a plate scale of 0.26 arcsec. The devices are arranged in the focal plane as an 8×8 pattern minus the four corner chips. The nominal focal plane is 418.88 mm in diameter or 3.0 degrees. With the gaps and masked regions, the 7.06 square degree FOV has an active region of about 5 square degrees. A description of the Pan-STARRS1 system is provided by Kaiser et al. (2010). The Pan-STARRS1 observations are obtained through a set of five broadband filters, which are designated as g_{P1} , r_{P1} , i_{P1} ,

Table 1. They have all been converted to rates per Mpc³ per Myr. The rate of GRBs are estimates of the true rates, after correction for the (uncertain) beaming factor. The distance columns refers to the distance within which the rates are calculated

Type	Rate Mpc ⁻³ Myr ⁻¹	Distance Mpc	Reference
Binary BH mergers	0.002-0.4	~400	Abbott et al. (2016b)
Core-collapse SN	96–140	30 – 400	Horiuchi et al. (2011); Li et al. (2011); Smartt et al. (2009)
Broad-lined Ic SN	1–4	30 – 400	Graham & Schady (2015); Kelly & Kirshner (2012); Smartt et al. (2009)
LGRBs (true)	0.1-0.6	≲450	Guetta & Della Valle (2007)
sGRBs (true)	1	≲400	Berger (2014)
Superluminous SN	0.01	900-2600	Quimby et al. (2011, 2013); McCrum et al. (2015)

z_{P1} , and y_{P1} . A further, broad filter w_{P1} , has been used primarily for near earth asteroid (NEO) searches (e.g. Veres et al. 2015) and is currently being employed in the NASA funded survey that produces both NEO discoveries and stationary transients (Huber et al. 2015a; Polshaw et al. 2015). Although the *griz*-band filter system for Pan-STARRS1 is similar to the SDSS (Abazajian et al. 2009), there are some significant differences. The g_{P1} filter extends 20 nm redward of the g_{SDSS} filter bandpass, which provides extra sensitivity but does include the 5577Å night sky emission line. The z_{P1} filter has a red cut off at 930 nm, whereas z_{SDSS} had a red response which was effectively defined by the detector efficiency. Pan-STARRS1 does not have a u -band, but extends redder to include a y_{P1} band, and has produced the first all sky image in this waveband. The Pan-STARRS1 photometric system is discussed in detail in Tonry et al. (2012b).

Images obtained by the Pan-STARRS1 system are processed with the Image Processing Pipeline (IPP) (see details in Magnier et al. 2013), originally on a computer cluster at the Maui High Performance Computer Center (MHPCC) but now located in Maui Research and Technology Center, Kihei, Maui. The pipeline runs the images through a succession of stages including device “de-trending”, a flux-conserving warping to a sky-based image plane, masking and artefact location (Waters et al. 2016, in prep.). De-trending involves bias and dark correction and flatfielding using white light flatfield images from a dome screen, in combination with an illumination correction obtained by rastering sources across the field of view. After determining an initial astrometric solution the flat-fielded images were then warped onto the tangent plane of the sky using a flux conserving algorithm. The warping to a sky-based image plane involves mapping the camera pixels to a defined set of sky-cells, of which there are approximately 51 per PS1 pointing. The plate scale for the warped images is 0.25 arcsec/pixel. Photometry from Pan-STARRS1 is in the “AB system” (see Tonry et al. 2012b, for a discussion) where the monochromatic AB magnitude is the logarithm of flux density

$$m_{AB}(\nu) = -2.5 \log(f_\nu / 3631 \text{ Jy}) \quad (1)$$

$$= -48.600 - 2.5 \log(f_\nu [\text{erg/sec/cm}^2/\text{Hz}]) \quad (2)$$

where $1 \text{ Jy} = 10^{-23} \text{ erg/sec/cm}^2/\text{Hz}$. The calibration of the Tonry et al. (2012b) PS1 photometric system through a reference star catalogue is described in detail in Schlafly et al. (2012) and Magnier et al. (2013). For the nightly processing, the zeropoints of the full-field camera chips are set from a catalogue of photometric reference stars from the “ubercal” analysis during the first reprocessing of all of the

PS1 3π data as described in Schlafly et al. (2012); Magnier et al. (2013). The internal calibration of this reference catalogue has a relative precision of around 1%. However the automated zeropoint applied in the difference imaging is currently an average full-field zeropoint calculated and this can lead to variations across sky-cells up to ± 0.15 .

The search for transients is greatly aided by having the pre-existing sky images from the Pan-STARRS1 Sky Surveys (Chambers et al 2016, in prep.) carried out by the PS1 Science Consortium. Transient sources are identified by the Image Processing Pipeline through analysis of difference images, created by subtracting the stacked image from the PS1SC 3π survey as a template from the observed image taken as part of the search for the counterpart. As described in Huber et al. (2015a) the g_{P1} , r_{P1} , i_{P1} , z_{P1} , and y_{P1} images employ the PS1 Science Consortium 3π reference stack (currently PV3 in the internal processing labelling) for difference imaging. The w_{P1} static sky stack is not available over the whole sky, but is employed where it exists on a nightly basis. Difference imaging by IPP has been further described in McCrum et al. (2014, 2015); Polshaw et al. (2015); Wright et al. (2015). Similar processing was implemented on the PS1 images discussed here and the imaging survey is further described in Section 3.1.

2.2 Spectroscopic instruments

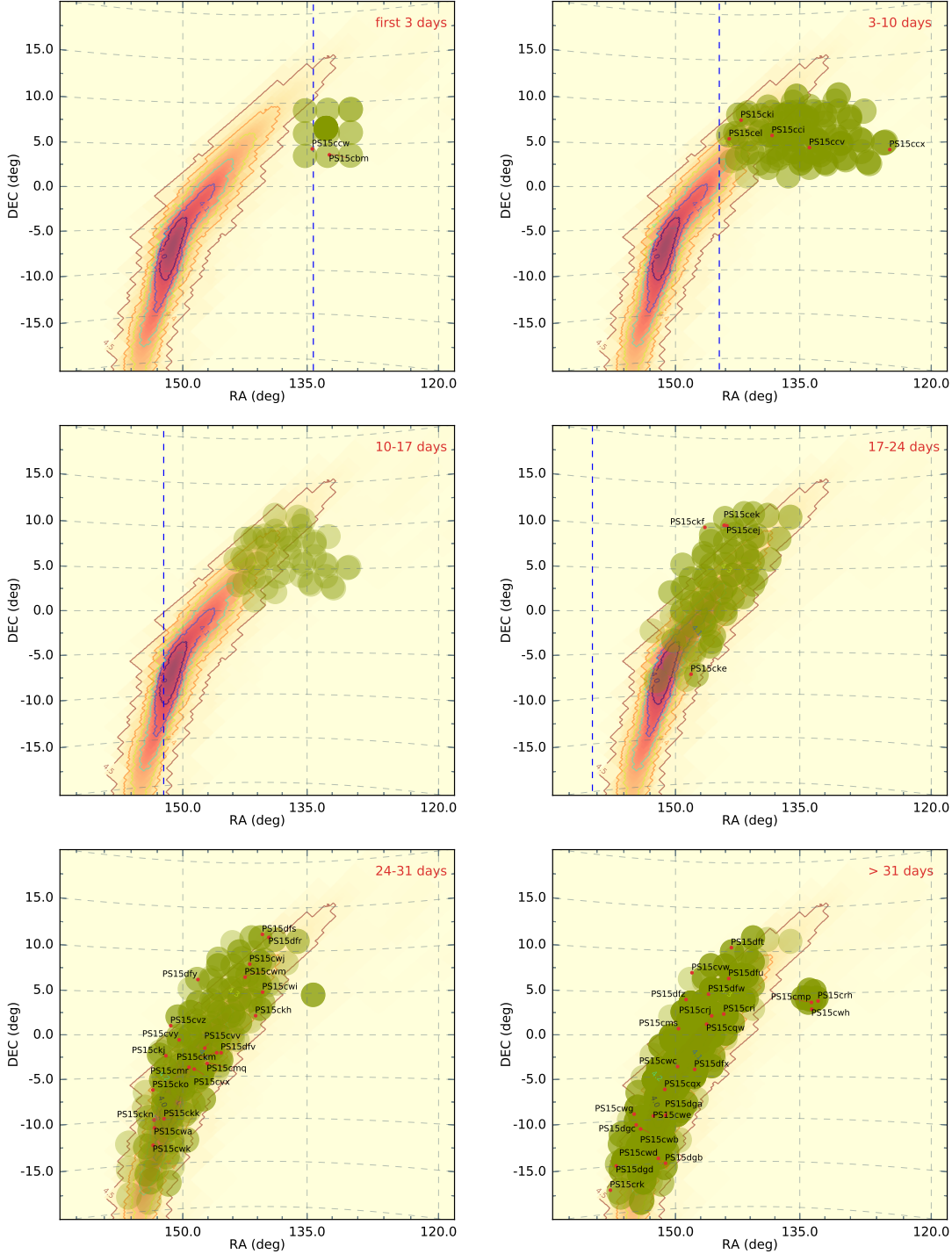
Spectroscopic follow-up was carried out with two main instruments, namely the SuperNovae Integral Field Spectrograph (SNIFS) on the University of Hawaii 2.2m Telescope (UH 2.2m) and the EFOSC2 spectrometer on the ESO New Technology Telescope (NTT) as part of the Public ESO Spectroscopic Survey of Transient Objects (PESSTO¹). One further spectrum was taken with the 200 inch Hale telescope at Palomar with the Double Spectrograph (DBSP).

2.2.1 SNIFS on the UH 2.2m telescope

SNIFS provides integral field spectra and was designed for supernovae spectroscopy (Lantz et al. 2004). It provides coverage over two arms : the blue covers 3200–5600Å at 2.4Å per pixel sampling and $R \simeq 1000$ at 4300Å; the red arm covers 5200-10000Å at 2.9Å per pixel sampling and $R \simeq 1300$ at 7600Å. The dichroic mirror which reflects light to the blue arm and transmits to the red has a cross-over region of 5000-5250Å within which it is difficult to recover reliable flux calibrated spectra during standard reductions. We hence chose

¹ www.pessto.org

Figure 1. Skymaps showing the probability contours produced by LIGO (solid contours), the PS1 pointings (green circles with diameters of 2.7° degrees and the positions of transients. The panels are separated into time intervals from discovery epoch of GW150914. A transient is plotted on the relevant panel if it was discovered in the epochs shown. All time is in the observer frame.



to remove this region in the spectra presented here. Data reductions were performed using the SNIFS SuperNova Factory (SNF) summit pipeline (Bacon et al. 2001; Aldering et al. 2006). Standard CCD processing included bias and flat-field corrections with images then converted into blue and red channel data cubes for bad pixel and cosmic-ray cleaning. Wavelength calibration used arc lamp exposures

taken at position of the target to minimise errors from telescope flexure and a rough flux calibration was applied using a historical response function for each data cube. A one-dimensional spectrum was extracted from each data cube using a point-spread function model with sky subtraction.

2.2.2 EFOSC2 on the NTT with PESSTO

The PESSTO survey is described in Smartt et al. (2015). The EFOSC2 spectrometer is employed on the ESO NTT at the nasmyth focus and Gr#13 is used to provide spectra between 3650-9250Å at a dispersion of 5.5Å pix⁻¹. A slit width of 1''0 is nominally used (unless poor seeing forces a change to 1''5) which results in a resolution of 18.2Å. All data presented in this paper were taken with a 1''0 slit. PESSTO employs a dedicated pipeline as described in Smartt et al. (2015), and all spectra were reduced using these standard procedures. The reduced spectra will be made public through the ESO Science Archive Facility during the summer of 2016, when the PESSTO project plans to release years 3 and 4 of the public survey in Spectroscopic Survey Data Release 3. Before then, all classification spectra will be placed on WISerEP ².

2.2.3 DPSP on the Hale

One spectrum was taken by T. Kupfer at the Palomar 200-inch Telescope (the Hale) using the Double Spectrograph (DBSP). This is a low to medium resolution spectrometer at cassegrain focus that uses a dichroic at 5500Å to split the beam and direct it to two separate red and blue channels. A 1''5 slit was used on the night of 25 Sep 2015 to observe one candidate (PS15cci, see Section 4) at airmass=2.627. The blue arm used the grating 600/4000 and the red arm had the 316/7500 grating installed, resulting in resolutions of approximately 4Å and 8Å FWHM respectively. Standard reduction procedures were employed to reduce the red and blue arms, including bias frame subtraction, extraction and sky subtraction, arc wavelength calibration and flux calibration (using the standard G191-B2B). A single good signal-to-noise spectrum (S/N~ 30 at 6000Å) resulted from the 1500s exposure time and the red and blue arms were merged for object classification.

3 THE PAN-STARRS OBSERVING CAMPAIGN OF LIGO SOURCE GW150914

GW150914 was announced to the collaborating groups who had offered dedicated observing facilities during the first observing run (O1) of LIGO on 16 September 2015 (06:39 UT) as source G184098. The source was detected by the LIGO Hanford Observatory and LIGO Livingston Observatory at 14 Sep 2015 09:50:45 UT (The LIGO Scientific Collaboration & the Virgo Collaborations 2015; Abbott et al. 2016b). Two sky maps were produced, one from the rapid localisation (the cWB map; Klimenko et al. 2016) and the other from the refined localisation (LALInference Burst : LIB, with date and time stamp 14 Sep 2015 19:02:54; Lynch et al. 2015)

A northern and southern sky banana shaped region was produced for each, with the 90% credible regions spanning about 700-800 square degrees. The night of the 16 Sep 2015 on Haleakala (05:00 - 15:00 UT) was wiped out due to poor weather and no Pan-STARRS observations took place. We started observing the G150914 northern banana on the night of 17 Sep 2015 (14:50 - 15:40 UT). Due to the RA location,

only the north western tip of the localisation banana was observable in the first 10 days, and at low airmass close to twilight. Figure 1 shows all the PS1 footprints (2.9 degrees diameter) in a binned time sequence and the probability sky contours from the final LIGO/Virgo LIB analysis.

During the first few days, we observed the cWB map region. This was due to us misinterpreting the time sequence of release and assuming the cWB was the more likely due to having a later date stamp from the LIGO/Virgo analysis. However this choice had little real effect as the more easterly, higher probability regions of the LIB analysis were inaccessible due their RA and indeed the first 3 day PS1 pointings shown in Figure 1 represent the eastern limits of the telescope's pointing capability at that time. As further illustrated in Figure 1, we stepped through the region in time to cover the bulk of the northern LIB localisation banana within 30-40 days. Pan-STARRS continued to observe this field until 26 October 2015 (MJD 57321). A combination of the r_{P1} , i_{P1} , z_{P1} and y_{P1} filters were used, for two reasons. One was that expected NS-NS mergers have predicted intrinsically red transients (Kasen, Badnell & Barnes 2013) and more practically, the sky brightness during the early observations (in astronomical twilight) forced a shift to the redder bands. The most common filter used was the i_{P1} -band. Exposure times were typically between 30-80 sec, and small dither strategies were employed to mitigate the fill factor problems of the GPC1 focal plane. A list of telescope pointings are available on request from the authors.

During subsequent analysis, the LIGO/Virgo team further refined the sky probability map, producing a final analysis result which they released to the collaborating teams as GCN 18858 (The LIGO Scientific Collaboration & the Virgo Collaboration 2015) and then publicly in (The LIGO Scientific Collaboration & the Virgo Collaboration 2016). The two maps released were BAYESTAR (Singer & Price 2016) and LALInference (?). The LALInference map with date stamp 2016 Jan 9, 1:29:46 was referred to "as the most accurate and authoritative localisation for this event" in GCN 18858, and described in detail in (The LIGO Scientific Collaboration & the Virgo Collaboration 2016). However this map favours the southern portion of the annulus originally released at the time we began follow-up, This resulted in a final 90 per cent credible region of 600 square degrees that was mostly in the south and a severe reduction in the northern probability. Hence our coverage is low, but this paper demonstrates the methods we have employed and will employ in the future to search for EM counterparts of GW sources.

We used i_{P1} , z_{P1} , y_{P1} band observations progressively to map as much of the GW150914 error region as possible due to the proximity of twilight. We have measured the boundaries of twilight in each of the PS1 filters where the end of evening twilight is defined as the time when the the sky brightness at constant altitude becomes constant, and the start of morning twilight is when the sky brightness ceases to be constant. For the PS1 $grizy_{P1}$ bands, this is when the sun is at 16, 16, 16, 14, and 10 degrees below the horizon at PS1 respectively (Chambers et al 2016, in prep). The proximity to twilight of the GW150914 error region limited the accessible RA at an hour angle of 4.5 hours or an airmass of approximately 2.6. Figure 1 shows the boundary of the accessible region in the i_{P1} band and Table Appendix X lists all the data.

² <http://wiserep.weizmann.ac.il/home>

Table 2. Transient candidates in the field of GW150914 (56 in total). Discovery dates refer to the date of the initial detection by Pan-STARRS. For reference, GW150914 was discovered at 20150914.41 (MJD 57279.41).

Name	RA (J2000)	Dec (J2000)	RA (J2000)	Dec (J2000)	Discovery Date	Discovery MJD	Disc mag.	Disc. flt.
PS15cbm	08 49 19.85	+03 48 17.8	132.33271	+3.80494	20150917.62	57282.62	18.55	<i>i</i> _{P1}
PS15ccw	08 57 30.60	+04 31 56.1	134.37750	+4.53225	20150917.63	57282.63	19.31	<i>i</i> _{P1}
PS15cci	09 13 22.76	+06 10 47.3	138.34483	+6.17981	20150919.63	57284.63	18.32	<i>i</i> _{P1}
PS15ccx	08 18 03.91	+04 18 04.2	124.51629	+4.30117	20150919.63	57284.63	19.42	<i>z</i> _{P1}
PS15ccv	08 55 23.05	+04 41 19.0	133.84604	+4.68861	20150922.62	57287.62	20.03	<i>i</i> _{P1}
PS15cel	09 34 11.58	+05 46 45.2	143.54825	+5.77922	20150923.63	57288.63	19.53	<i>i</i> _{P1}
PS15cki	09 28 27.24	+08 00 51.5	142.11350	+8.01431	20150923.64	57288.64	19.17	<i>z</i> _{P1}
PS15cej	09 35 19.41	+10 11 50.7	143.83087	+10.19742	20151002.62	57297.62	18.13	<i>i</i> _{P1}
PS15cek	09 36 41.04	+10 14 16.2	144.17100	+10.23783	20151002.63	57297.63	17.24	<i>z</i> _{P1}
PS15cke	09 52 35.14	-07 36 32.0	148.14642	-7.60889	20151002.64	57297.64	16.72	<i>z</i> _{P1}
PS15ckf	09 45 57.71	+09 58 31.4	146.49046	+9.97539	20151003.65	57298.65	17.57	<i>y</i> _{P1}
PS15cwj	09 27 44.89	+08 31 32.1	141.93704	+8.52558	20151013.60	57308.60	20.02	<i>i</i> _{P1}
PS15cwi	09 21 31.27	+05 10 26.8	140.38029	+5.17411	20151013.61	57308.61	20.43	<i>i</i> _{P1}
PS15ckm	09 43 47.15	-02 10 13.3	145.94646	-2.17036	20151013.61	57308.61	19.57	<i>i</i> _{P1}
PS15ckj	10 07 58.59	-02 29 47.9	151.99412	-2.49664	20151013.61	57308.61	18.31	<i>i</i> _{P1}
PS15cko	10 14 01.69	-06 30 46.9	153.50704	-6.51303	20151013.62	57308.62	19.51	<i>i</i> _{P1}
PS15ckh	09 24 55.83	+02 19 25.1	141.23263	+2.32364	20151013.62	57308.62	19.40	<i>i</i> _{P1}
PS15cvz	10 05 41.49	+01 05 33.2	151.42288	+1.09256	20151013.62	57308.62	19.55	<i>i</i> _{P1}
PS15cvy	10 01 45.13	-00 36 06.8	150.43804	-0.60189	20151013.63	57308.63	19.76	<i>i</i> _{P1}
PS15ckn	10 13 29.31	-10 00 06.1	153.37213	-10.00169	20151014.62	57309.62	19.44	<i>i</i> _{P1}
PS15ckk	10 08 48.60	-09 54 50.7	152.20250	-9.91408	20151014.62	57309.62	16.43	<i>i</i> _{P1}
PS15dfs	09 21 37.60	+12 01 38.0	140.40667	+12.02722	20151015.60	57310.60	20.94	<i>i</i> _{P1}
PS15dfr	09 18 29.04	+11 40 10.4	139.62100	+11.66956	20151015.60	57310.60	21.31	<i>i</i> _{P1}
PS15cwm	09 30 01.03	+06 58 12.6	142.50429	+6.97017	20151015.61	57310.61	20.90	<i>i</i> _{P1}
PS15dfy	09 52 48.76	+06 38 04.5	148.20317	+6.63458	20151015.61	57310.61	19.82	<i>i</i> _{P1}
PS15evv	09 49 30.25	-01 36 37.5	147.37604	-1.61042	20151015.62	57310.62	20.14	<i>i</i> _{P1}
PS15cmr	09 57 03.59	-03 53 24.3	149.26496	-3.89008	20151015.62	57310.62	19.35	<i>i</i> _{P1}
PS15cmq	09 48 22.97	-03 27 41.4	147.09571	-3.46150	20151015.62	57310.62	20.19	<i>i</i> _{P1}
PS15cvx	09 54 35.48	-04 07 22.3	148.64783	-4.12286	20151015.62	57310.62	20.32	<i>i</i> _{P1}
PS15dfv	09 41 38.31	-02 10 21.8	145.40963	-2.17272	20151015.62	57310.62	20.83	<i>i</i> _{P1}
PS15cwa	10 13 18.75	-10 54 43.9	153.32812	-10.91219	20151015.63	57310.63	20.27	<i>i</i> _{P1}
PS15cwk	10 13 55.42	-12 52 49.2	153.48092	-12.88033	20151015.63	57310.63	20.11	<i>i</i> _{P1}
PS15cms	09 58 35.10	+00 44 34.7	149.64625	+0.74297	20151017.62	57312.62	19.93	<i>i</i> _{P1}
PS15cvw	09 52 09.25	+07 26 48.3	148.03854	+7.44675	20151018.61	57313.61	19.86	<i>i</i> _{P1}
PS15cmp	08 54 24.40	+03 54 00.5	133.60167	+3.90014	20151019.58	57314.58	21.82	<i>r</i> _{P1}
PS15crh	08 51 16.19	+04 03 57.9	132.81746	+4.06608	20151019.58	57314.58	21.39	<i>r</i> _{P1}
PS15cwh	08 54 15.18	+03 04 59.0	133.56325	+3.08306	20151019.58	57314.58	22.09	<i>r</i> _{P1}
PS15cri	09 36 50.66	+02 31 20.0	144.21108	+2.52222	20151021.60	57316.60	20.67	<i>i</i> _{P1}
PS15cwb	10 16 21.58	-11 00 10.5	154.08992	-11.00292	20151021.61	57316.61	20.25	<i>i</i> _{P1}
PS15dgc	10 18 20.86	-10 31 28.3	154.58692	-10.52453	20151021.61	57316.61	20.42	<i>i</i> _{P1}
PS15cwe	10 10 24.74	-09 33 10.0	152.60308	-9.55278	20151021.63	57316.63	20.47	<i>i</i> _{P1}
PS15crk	10 30 03.48	-17 31 38.7	157.51450	-17.52742	20151021.63	57316.63	19.97	<i>i</i> _{P1}
PS15dgb	10 04 43.54	-15 00 03.8	151.18142	-15.00106	20151021.63	57316.63	20.71	<i>i</i> _{P1}
PS15dga	10 04 42.37	-09 31 14.8	151.17654	-9.52078	20151021.63	57316.63	20.34	<i>i</i> _{P1}
PS15dfx	09 50 52.07	-04 09 46.3	147.71696	-4.16286	20151023.60	57318.60	20.80	<i>i</i> _{P1}
PS15cwg	10 19 19.55	-09 16 01.2	154.83146	-9.26700	20151023.61	57318.61	20.39	<i>i</i> _{P1}
PS15crj	09 42 42.16	+02 18 09.8	145.67567	+2.30272	20151023.62	57318.62	20.88	<i>i</i> _{P1}
PS15dfz	09 54 59.64	+04 14 08.1	148.74850	+4.23558	20151023.62	57318.62	20.68	<i>i</i> _{P1}
PS15dfu	09 34 24.28	+06 48 01.0	143.60117	+6.80028	20151023.62	57318.62	21.19	<i>i</i> _{P1}
PS15dft	09 33 09.38	+10 28 02.2	143.28908	+10.46728	20151023.62	57318.62	19.41	<i>i</i> _{P1}
PS15dfw	09 44 11.65	+04 54 52.1	146.04854	+4.91447	20151024.60	57319.60	21.00	<i>i</i> _{P1}
PS15cwc	09 59 01.22	-03 48 04.3	149.75508	-3.80119	20151024.61	57319.61	21.11	<i>i</i> _{P1}
PS15cqx	10 05 03.70	-06 29 44.7	151.26542	-6.49575	20151024.61	57319.61	20.32	<i>i</i> _{P1}
PS15dgd	10 27 26.07	-14 58 20.1	156.85862	-14.97225	20151024.61	57319.61	20.55	<i>i</i> _{P1}
PS15cqw	09 45 06.43	+01 17 02.0	146.27679	+1.28389	20151025.60	57320.60	20.99	<i>i</i> _{P1}
PS15c wd	10 08 06.70	-14 25 08.5	152.02792	-14.41903	20151025.62	57320.62	20.93	<i>i</i> _{P1}

Table 3. Classifications of all transient candidates in the field of GW150914. Discovery dates refer to the date of the first detection by Pan-STARRS. “Spec. date” refers to the date of the classification spectrum. The Type designation of (SN) means that a spectrum was not available, but the absolute magnitude and lightcurve data available are consistent with a normal supernova. The instrument or survey data are listed in “Notes” and described in the text. Some objects have no classification spectrum, but have spectroscopic host redshifts from NED. “Phase Spec.” refers to the estimated phase of the spectrum with respect to peak. “Exp. Date” refers to the estimated time of the explosion of the supernova (from the spectroscopic typing information) with respect to the time of GW150914 (the day of 14 Sep 2015) e.g. -17d means the SN is estimated to have exploded 17 days before GW150914. The uncertainties are discussed in the text.

Name	Disc. Date	Spec Date	Type	Phase Spec	Spec z	Exp. Date	Notes
PS15cbm	20150917.62	20151003	SN Ia	>20d	0.059	-17d	PESSTO
PS15ckm	20151013.61	20151022	SN Ia	peak	0.080	+20d	UH2.2m+SNIFS
PS15cwm	20151015.61	...	(SN)	...	(0.22)	...	SDSS DR12 photo- z , association uncertain
PS15ccw	20150917.63	...	(SN)	...	0.072	...	host z , SDSS DR12
PS15cci	20150919.63	20150926	SN Ia	pre-peak	0.055	-1d	DBSP, SN1991T-like
PS15ccx	20150919.63	20150927	SN Ia	15-20d	0.097	-25d	GCN18371 , LT+SPRAT
PS15ccv	20150922.62	...	(SN)	...	0.071	...	host z , SDSS DR12
PS15cel	20150923.63	20151012	SN II	> 20d	0.057	-2d	PESSTO
PS15cki	20150923.64	20151020	SN II	> 25d	0.024	+6d	UH2.2m+SNIFS
PS15cej	20151002.62	20151010	SN Ia	peak	0.049	+8d	PESSTO
PS15cek	20151002.63	...	AGN	...	0.060	...	2MFGC 7447, SDSS DR12 spectrum
PS15cke	20151002.64	20151014	SN Ia	50d	0.030	-38d	UH2.2m+SNIFS
PS15ckf	20151003.65	20151020	SN II	>15d	0.019	+13d	UH2.2m+SNIFS
PS15cwj	20151013.60	20151117	SN Ia	21d	0.135	+25d	PESSTO
PS15cwi	20151013.61	20151118	SN II	+30d	0.058	+32d	PESSTO
PS15ckj	20151013.61	20151022	SN II	peak	0.020	+33d	UH2.2m+SNIFS, in IC593 $z = 0.02018$
PS15cko	20151013.62	20151025	SN II	post-peak	0.217	uncertain	SNIFS,PESSTO
PS15ckh	20151013.62	...	QSO	...	1.523	...	Lensed QSO [IBB2003] J0924+0219
PS15cvz	20151013.62	...	(SN)	...	0.069	...	host z , SDSS DR12
PS15cvy	20151013.63	20151022	SN II	young	0.046	+ 33d	UH2.2m+SNIFS
PS15ckn	20151014.62	20151027	SN Ic	+7d	0.08	+23d	UH2.2m+SNIFS
PS15ckk	20151014.62	...	AGN	...	0.058	...	NPM1G-09.0361
PS15dfr	20151015.60	...	(QSO)	...	(0.549)	...	Coincident with MLS140206-091829+114011
PS15dfs	20151015.60	...	(SN)	...	(0.424)	...	Offset from host galaxy, SDSS DR12 photo- z
PS15dfy	20151015.61	...	(QSO)	...	(0.582)	...	Likely QSO, MLS130216-095249+063804
PS15cvv	20151015.62	...	(SN)	hostless
PS15cmr	20151015.62	20151027	SN Ia	+7d	0.093	+18d	UH2.2m+SNIFS , host $z = 0.093$ SDSS DR12
PS15cmq	20151015.62	20151117	SN II	+11d	0.065	+48d	PESSTO
PS15cvx	20151015.62	...	(SN)	...	0.152	...	host spec- z 2dFGRS
PS15dfv	20151015.62	...	(QSO)	Likely QSO SDSS J094138.31-021021.7
PS15cwa	20151015.63	...	(SN)	3''9 from host galaxy
PS15cwk	20151015.63	...	(SN)	15''4 from host galaxy
PS15cms	20151017.62	20151024	SN Ia	peak	0.065	+22d	UH2.2m+SNIFS
PS15cvw	20151018.61	...	(SN)	faint, $r = 22.7$ host galaxy
PS15cmp	20151019.58	...	(SN)	...	0.097	...	host z , SDSS DR12
PS15scrh	20151019.58	...	(SN)	faint, $r = 21.9$ host galaxy
PS15cwh	20151019.58	...	(SN)	old	0.028	...	host z , SDSS DR12, old
PS15cri	20151021.60	...	(SN)	hostless
PS15cwb	20151021.61	20151121	SN Ia	+20d	0.145	+30d	PESSTO
PS15dgc	20151021.61	...	(SN)	...	0.056	...	Offset 6''6 from host, spec- z in NED
PS15cwe	20151021.63	...	(SN)	hostless
PS15crk	20151021.63	...	(SN)	6''5 from host galaxy
PS15dga	20151021.63	...	(SN)	Offset from host galaxy
PS15dgb	20151021.63	...	(SN)	Offset from host galaxy in PS1
PS15dfx	20151023.60	...	(SN)	Offset from host galaxy in PS1
PS15cwg	20151023.61	...	(SN)	0''7 from host galaxy
PS15crj	20151023.62	...	(SN)	...	(0.41)	...	1''9 from host galaxy, SDSS DR12 photo- z
PS15dft	20151023.62	...	CV	Known CV, ASASSN-15se
PS15dfu	20151023.62	...	(SN)	...	0.0866	...	2''7 from host galaxy SDSS DR12 spec- z
PS15dfz	20151023.62	...	QSO	...	0.844	...	QSO, SDR12 spectrum
PS15dfw	20151024.60	...	(SN)	...	(0.113)	...	Offset from host galaxy SDSS, DR12 photo- z
PS15cwc	20151024.61	...	(SN)	hostless
PS15cqx	20151024.61	...	(SN)	...	0.054	...	host z from NED
PS15dgd	20151024.61	...	(SN)	Offset 5''6 from host
PS15cqw	20151025.60	...	(SN)	...	(0.22)	...	1''9 from host galaxy, SDSS DR12 photo- z
PS15c wd	20151025.62	...	(SN)	5''5 from host galaxy

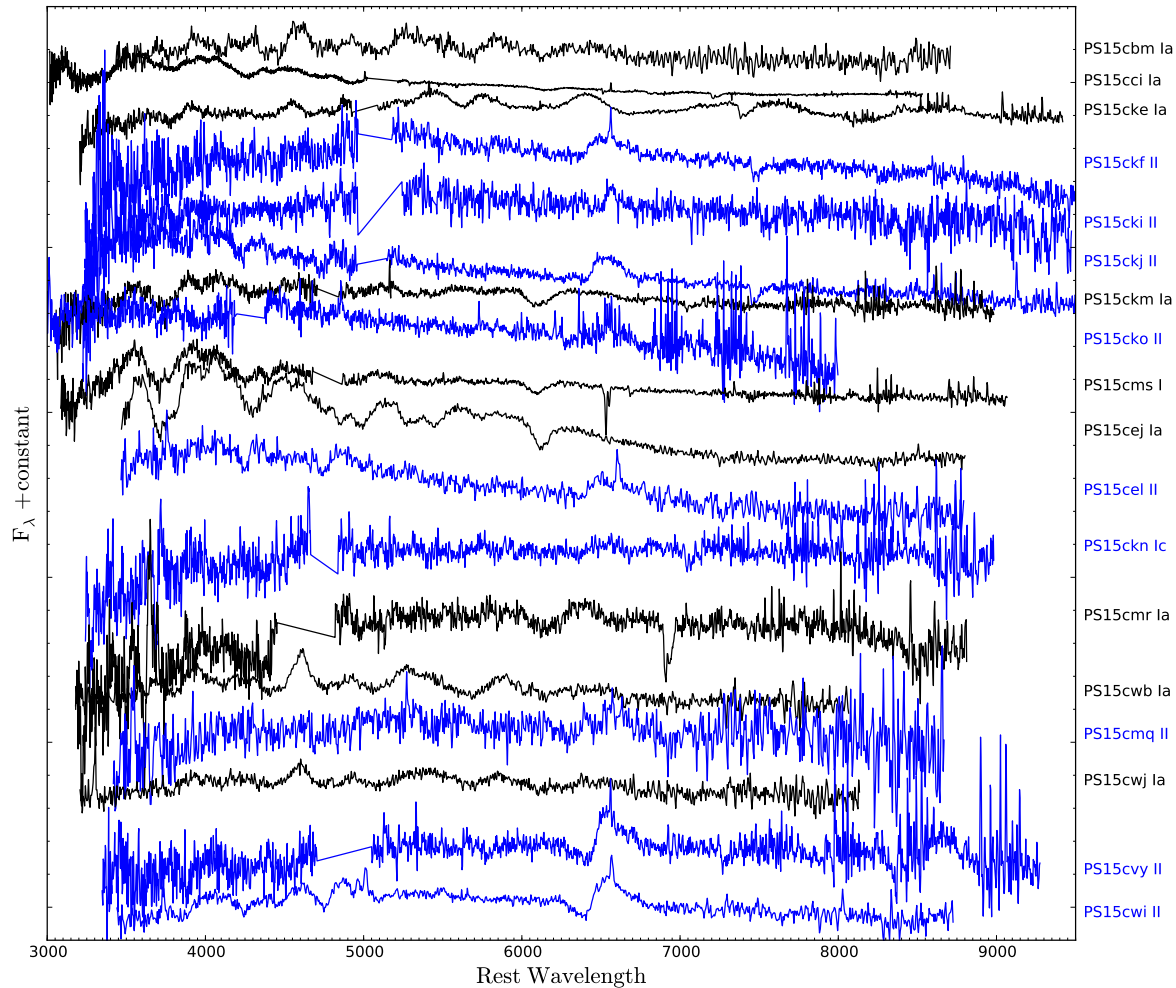


Figure 2. Spectra of all the candidates for which data were taken. The type Ia, and likely type Ia are shown in black, and the core-collapse SNe are shown in blue.

3.1 The search for transients in the Pan-STARRS1 fields

The PS1 3π stack in the r_{iZyP1} filters was used as the reference image to perform image subtraction on each of the images taken by Pan-STARRS during the campaign described in Section 3. Each of the individual frames were differenced, and no stacks of overlapping frames (due to small dithers) were used. The difference images were processed by the IPP in Hawaii, producing catalogues of potential astrophysical transients. As normal with CCD based difference image surveys, the false positives introduced by the processing outweigh the real objects by 2-3 orders of magnitude (e.g. Brink et al. 2013; Wright et al. 2015; Goldstein et al. 2015). The following lists the steps taken during our filtering of this data stream. In total 10,173,434 difference detections were processed.

- Pre-database rejection : during the database ingest process objects from the detection catalogues are rejected which have any one of 10 poor quality FLAGS set by IPP. These image quality flags are determined by IPP and are a fairly robust way of removing artefacts by detecting saturated and

defective pixels, inconsistent sky variance, and objects for which the XY moments can not be determined or which have very poor point-spread-function fits. All objects without any of these FLAGS set are ingested into the Transient Science Server Database (a MySQL relational database). The FLAG check resulted in the rejection of 5,133,123 difference detections. The remaining 5,040,311 detections were ingested into the MySQL database. Detections within 0.5 arcsec of other detections are aggregated into objects which resulted in the creation of 3,060,121 distinct objects.

- To further restrict the numbers, we require a minimum of 2 separate detections on separate images each with a signal-to-noise greater than 3σ and a value for $MOMENTS_XY < 3.6$ (the second moment in xy). The two detections must be within $0''.5$ separation and the RMS of positional scatter (of all detections) must be $\leq 0''.25$. This immediately helps remove any uncatalogued minor planets that move between two images, cosmic ray hits and some types of artefacts.

- Like most CCD mosaic arrays, the giga-pixel camera (GPC1) suffers from cross-talk, such that bright stars cause electronic ghost (PSF-like) sources on other cells and arrays

with well known rules. The size of the FOV means that the number of bright stars that cause such cross-talk ghosts is significant and care must be taken to identify them. The IPP checks and sets an `ON_GHOST` flag if an object has a parent bright star at a known cross-talk position. If an object has this flag set on any one detection, then it is rejected.

These basic checks, and an insistence of 2 separate detections resulted in a total of 308,262 objects which were labelled as candidate astrophysical transients in the Transient Science Server database. To further refine the search, the following filters were applied.

- The ratio of positive, negative and NaN (masked) pixels within an object aperture is used to reject objects with significant numbers of negative or masked pixels. This efficiently removes “dipoles” which come from convolution artefacts during differencing. The current thresholds are set as below, where $nPos$ = number of positive pixels, $fPos$ = flux from positive pixels within the aperture (similar definitions for $nNeg$ and $fNeg$)

- $\text{diff_npos} = nPos > 3$
- $\text{diff_fratio} = fPos/(fPos + fNeg) > 0.6$
- $\text{diff_nratio_bad} = nPos/(nPos + nNeg) > 0.4$
- $\text{diff_nratio_mask} = nPos/(nPos + nMask) > 0.4$
- $\text{diff_nratio_all} = nPos/(nPos + nMask + nNeg) > 0.3$

- All objects within $1''.0$ of a catalogued star in the 2MASS Point source Catalogue, the Guide Star Catalogue and a PS1 stellar catalogue (taken from an extended uber-catalogue based on Schlafly et al. 2012; Finkbeiner et al. 2015) were rejected. The 1 arcsec search radius was used for 2MASS, GSC and PS1 Ubercal stars. For the SDSS star catalog we varied the association radius between 19 (for an $r = 13$ star) and 2.5 arcsec (for an $r = 18$ star).

- All objects within a variable radius of very bright stars are rejected, as likely diffraction spikes, saturation bleeds or other optical effects. The radius of this mask applied is magnitude dependent varies from 15 to 40 arcsec for stars between 8 to 13 magnitudes. We typically lose about 0.5 per cent of the sky area to this bright star masking.

These three filters reduced the number of objects to 48,550. The Transient Science Server then located 300×300 pixel postage stamp image data for all these objects that pass the above filters. We also cross match against the Minor Planet Centre and identify known movers. Although the requirement of a positional scatter of $RMS < 0''.25$ inherently removes many movers, there are some slow moving objects that get through this filter and these real, slow movers are useful for consistency checks on the image analysis that follows (in this case there were only 3 known slow movers that made it this far). A machine learning algorithm was run on these pixel stamps that calculates a real-bogus factor between 0 (bogus) and 1 (real) as described in Wright et al. (2015). The machine learning algorithm employed for PSST (Huber et al. 2015a) is similar in concept to that described in Wright et al. (2015) but has now been revised to be a Convolutional Neural Network, based on the approach of Ngiam et al. (2011) and further details are available in (Wright 2015). For completeness, the threshold cut was chosen such that the machine allowed 10 per cent false positives and 1 per cent missed detections. The resulting number of objects

remaining for human inspection was 5,861. This resulted finally in 56 transients which had high real-bogus factors which we confirm as real astrophysical objects. We found a further 71 faint, more marginal objects that were either coincident with known AGN (in the catalogue of Véron-Cetty & Véron 2001) or coincident with candidate AGN/QSOs from the MILLIQUAS catalogue³ (Flesch 2015), or coincident with faint stars, or had faint detections on only one night. These are likely to be a combination of low-level AGN or stellar variability, faint movers, or in some cases convolution artefacts occurring when the image quality was sharper than the reference stack. They may also be faint SNe that were only detected on one night. We consider these as dubious objects for which we could not be certain they were of astrophysical origin and a list is available on request.

4 RESULTS OF TRANSIENTS LOCATED

Of the 56 transients that we detected, a total of 19 were observed spectroscopically. 18 spectra are presented in this paper, with one classification from a GCN announcement by Steele, Copperwheat & Piascik (2015). A further 13 have archival spectra of the host galaxies, providing host redshifts (with 4 of them being known AGN/QSOs⁴). The spectroscopic classifications and host redshifts are listed in Table 3. All transients appear to be normal population supernovae/AGN/QSOs that we would expect to detect in the Pan-STARRS1 survey fields (together with 1 CV). In the following subsections, we discuss the transients with and without direct spectroscopic confirmation and classification. Throughout the analysis we use $H_0 = 72 \text{ km s}^{-1} \text{ Mpc}^{-1}$, $\Omega_M = 0.3$, $\Omega_\Lambda = 0.7$.

4.1 Spectroscopically classified transients

Table 3 lists the spectroscopic classifications of the 19 transients for which spectra were taken. We find ten type Ia SNe, eight type II SNe, one type Ic. None of these candidates could be immediately linked to a GW signal and none are markedly peculiar. They appear to be typical SNe that are discovered and spectroscopically classified in wide-field surveys.

The spectra of these supernovae allow estimations of the explosion epochs. We estimate the explosion epochs from matching the observed spectra with template spectra in both the supernova spectral matching tools SNID (Blondin & Tonry 2007) and Gelato (Harutyunyan et al. 2008). Uncertainties in these values vary depending on the spectral type and the availability of good templates. Where we quote uncertainties below these are the epoch ranges that are reasonably matched to the spectra. Anderson et al. (2014) showed that such spectral matching gives consistent results to lightcurve data with non-detections. If any transient or

³ <http://heasarc.gsfc.nasa.gov/w3browse/all/milliquas.html>

⁴ These 4 were high significance transients that we kept in our good catalogue in case they showed any sign of being circumnuclear transients rather than AGN/QSO variability. We put the other faint and marginal sources which were coincident with candidate AGN/QSO in the 71 possible sources, as we were uncertain if they were real or difference image artefacts.

supernova were to be plausibly linked to a GW trigger, then one would reasonably expect that the explosion epoch would be close in time to that of the GW detection time. From the classification phase of the spectrum, we can approximately estimate the time of explosion of the SNe and find that all but three or four have estimated explosion epochs more than 2 weeks before or after the time of GW150914. The types and epochs as listed in Table 3 are therefore mostly unremarkable. There are 5 transients worth some further discussion and we provide specific sections on these below, while the rest are effectively discounted from being related and the information is available in Table 3.

4.1.1 PS15cci

PS15cci was discovered as a rising transient in a relatively faint and compact host galaxy (SDSS J091322.78+061047.6, $r = 19.78 \pm 0.03$) with a photometric redshift of $z = 0.08 \pm 0.04$. It was found in the first few days of our searching (19 Sept 2015, or 4 days after the trigger) and the rising nature immediately caught our attention. We classified it as a type Ia SN on 26 Sept 2015 (with a high S/N spectrum from the Palomar 200 inch and the DBSP spectrometer), with a spectroscopic age of roughly 4 ± 4 days before maximum light, at $z = 0.055$. This means that assuming a rise-time of 18 ± 2 days from explosion to maximum light for type Ia SNe (Ganeshalingam, Li & Filippenko 2011) our estimated explosion epoch is -1 ± 6 d from the detection of GW150914. The explosion epoch of PS15cci is broadly consistent with that of GW150914, but being a normal type Ia, at $z = 0.055$ (although resembling the bright SN1991T-like subclass; Phillips et al. 1992; Filippenko 1997) we discount it as being related.

4.1.2 PS15cel

PS15cel was discovered on 23 Sept 2015 (9 days after the GW source detection), with a spectrum taken by PESSTO on 12 Oct 2015. It is a type II with a broad and narrow component of $H\alpha$. The narrow component is very likely from the host galaxy (SDSS J093411.53+054644.7) which we measure at $z = 0.057$. The lightcurve is plotted in Fig. 3 and is fairly flat in the first 30 days. All photometric points on the lightcurve are from PS1 apart from one set of $BVRiz$ taken with EFOSC2 as part of PESSTO (see Smartt et al. 2015, for a description of the filters). The transient reaches a peak mag of $i_{P1} = -18.0$ mag assuming only foreground Milky Way extinction. The plateau phase is observed to last at least 85 days, which is not unusual for a II-P SN, although the more luminous type II events tend to have faster decline rates as shown by the recent work of Anderson et al. (2014) and Galbany et al. (2016). PS15cel is in the regime of the brightest type II SNe known, as defined by the Anderson et al. sample, and also declines relatively slowly (at 0.6 mag per 100d in the i_{P1} band). While it sits on the edge of the brightness vs decline rate plot as defined in Fig. 7 of Anderson et al. (2014) it is not a far enough from this locus to be an outlier. It is also not an outlier in the peak magnitude vs Δm_{15} relation for type II SNe of Rubin et al. (2015). The last point in the r -band shows the SN is dropping off the plateau onto the nebular, tail phase which is powered by the

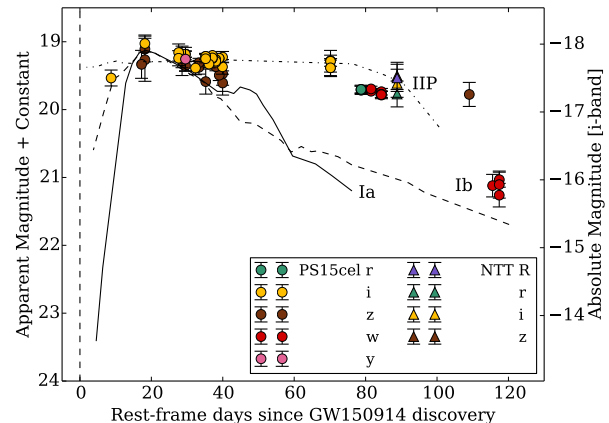


Figure 3. The lightcurve of PS15cel with all data points in the PS1 photometric system. Five points were taken in the PS1 w -band during routine PSST operations and can be considered to be similar to r_{P1} (as seen in the close agreement at 80 days). The PESSTO riz points (at +75d) were also transformed to the PS1 AB mag system for meaningful comparison. The right hand axis shows the absolute magnitudes in the i_{P1} -band (the other filters can be considered similar, apart from the small differences in foreground extinction between the bands).

decay of ^{56}Co , which is again normal behaviour for luminous type II SNe (e.g. Inserra et al. 2013a).

The PESSTO spectrum taken on 12 Oct 2015 (19 days after discovery) is plotted in Fig. 2. The P-Cygni absorption troughs of the Balmer line series are weak, and the normal Fe II lines have not become prominent. The spectrum resembles type II-P SNe at a few days past explosion (SN2004et, SN1999em and SN2006bp), but the Pan-STARRS lightcurve clearly dates the SN at least 19 days after explosion. This SN bears some resemblance to the bright and luminous type II SNe SN1992H and SN2009kf (Botticella et al. 2010; Clocchiatti et al. 1996) for which Utrobin, Chugai & Botticella (2010) have proposed explosion energies of 2×10^{52} ergs, ejecta masses of $\sim 30M_{\odot}$ and ^{56}Ni masses of $\sim 0.4M_{\odot}$. To produce such an energetic explosion in a very massive star, Utrobin, Chugai & Botticella (2010) proposed a rapid disk accretion onto a central black hole at the time of core-collapse. Although the time of discovery was 23 Sept 2015, 9 days after GW150914, we do not have data to rule out that the SN exploded before the discovery date and indeed the flat plateau would suggest that it did. Type II have rise times ranging from 5-10 days (Gall et al. 2015; González-Gaitán et al. 2015; Rubin et al. 2015) and as we did not detect that rise time, an explosion date close to the epoch of GW150914 is quite possible. Although the rapid disk accretion onto a central black hole model of Utrobin, Chugai & Botticella (2010) does involve a massive compact remnant it is certainly not quantitatively similar to the BH-BH merger that is proposed for GW150914 (Abbott et al. 2016b). Therefore one could not reasonably link the two on the basis of the data in hand and the predictions for the GW signal from massive asymmetric core collapse realistically sets the distance limits at 10-50 Mpc (Piro & Thrane 2012).

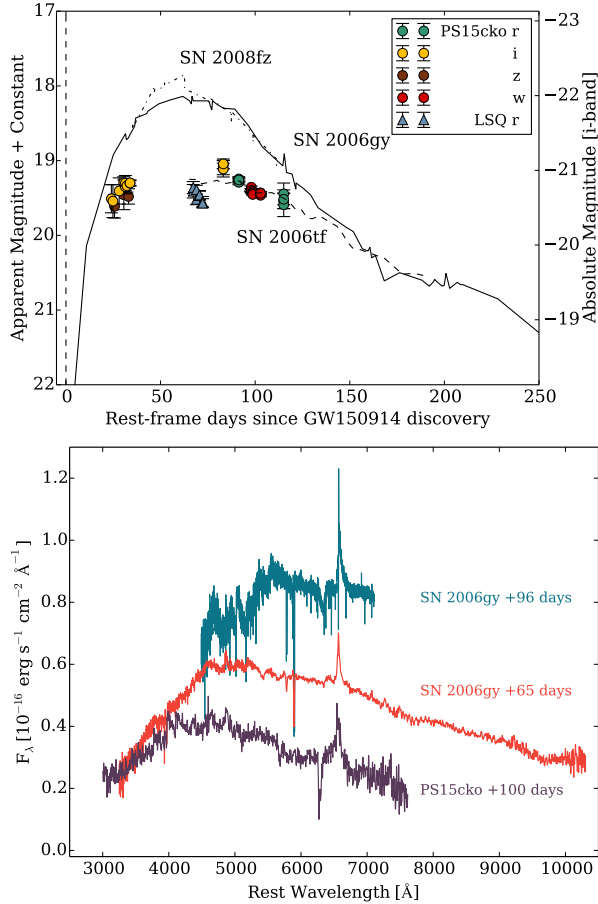


Figure 4. Top : The lightcurve of the luminous PS15cko compared to two three other superluminous type II_n SNe. No host reddening has been applied to PS15cko. **Bottom:** Spectral comparison of PS15cko with the two spectra of SN2006gy. Each spectrum has been corrected for foreground extinction only, since the host extinction to PS15cko is uncertain. The lightcurves and spectral comparison indicate this is a luminous type II_n SN.

4.1.3 PS15cki

This is offset by $3''.3$ from a faint diffuse host galaxy visible in the PS1 reference image and measured as $r = 19.91 \pm 0.11$ in SDSS DR12 (SDSS J092827.13+080048.6). The spectrum is low signal-to-noise, but a broad $H\alpha$ line is visible indicating a type II SN with an age around 30 ± 10 days after explosion. This would put the explosion epoch at about $\text{MJD} = 57285 \pm 10$ which broadly covers the GW150914 detection at $\text{MJD} = 57279.41$. However the absolute magnitude of $M_i = -16.1$ and redshift of $z = 0.024$ imply this is a fairly normal type II SN in a faint host galaxy and unrelated to the GW burst

4.1.4 PS15ckn

The SNIFS spectrum is of moderate quality with fairly low signal ($S/N \sim 10$ after binning to 10\AA per pixel), but the spectrum can be classified as a type Ic SN at about 7 ± 3 days after maximum light. Type Ic SNe have rise times of around 14 ± 5 days (Valenti et al. 2011; Taddia et al. 2015; Prentice et al. 2016) hence the explosion date of this can be esti-

mated at $\text{MJD} = 57302 \pm 8$, which is around 23 ± 8 days after GW150914. While some broad lined type Ic SNe are associated with GRBs (Woosley & Bloom 2006) and black hole formation, PS15ckn does not appear to be a broad lined or energetic Ic. At a redshift of $z = 0.08$, our brightest measured magnitude is $M_i = -18.4$ which implies it is not unusually luminous. The SN is $2''.9$ from the core of a spiral galaxy (probably SA-SB type in the PS1 images) which is also a UV source (GALEXASC J101329.20-100003.6). In conclusion, the data we have suggests PS15ckn unlikely to be unrelated to the GW source.

4.1.5 PS15cko

A spectrum was taken with SNIFS on 2015 October 25, which was 12 days after the discovery. The signal to noise is low and the redshift is not securely determined from either broad lines from the transient or narrow lines from the host galaxy. There is a resolved host galaxy in the PS1 image reference stack separated by $3''.4$ which is likely the host. The spectrum is shown in Fig.2, has no strong and distinct features. The lightcurve shows that when it was discovered on 2015 October 13, it continued to rise in the i and z -bands for about 12 days. The discovery date is already 29 days after GW150914, so for it to be related would require a very long rise time which would be in the regime of superluminous SNe (Nicholl et al. 2015) or very bright type II_n explosions (Smith et al. 2007).

It was recovered in both routine La Silla QUEST Baitay et al. (2013) and PSST (Huber et al. 2015a,b) operations on $\text{MJD} = 57361$ to 57419, more than 100 days past first discovery and still relatively bright at $i_{P1} = 20$ and $r_{LSQ} = 19.4$ (LSQ filter has a broad optical filter and this mag is approximately an AB r -mag equivalent). A PESSTO spectrum taken on 4 Feb 2016 conclusively sets it at $z = 0.217$, with a very strong $H\alpha$ line profile in emission. Figure 4 shows that this is likely a luminous SN II_n. The initial peak means a restframe r -band magnitude of $M_r = -20.6$, assuming the observer frame i_{P1} transforms to the r -band with a nominal k -correction of $2.5 \log(1+z)$. Figure 4 shows the lightcurve comparisons with SN2006gy, SN2006tf and SN2008fz (data from Smith et al. 2007; Ofek et al. 2007; Smith et al. 2008; Drake et al. 2010). The explosion epoch is uncertain. The lightcurve implies it was probably after GW150914 but the range in uncertainty is large enough that it could be compatible. We currently discount this as related to GW150914 on three counts. There are no plausible models linking II_n SNe to GW production, it is much further than the estimate for GW150914 and the explosion epoch is not obviously compatible with the time of GW150914.

4.1.6 PS15ccx

This was discovered on $\text{MJD} = 57284.63$ at $z_{P1} = 19.42 \pm 0.14$. A resolved host galaxy is visible in SDSS and the PS1 stack, at $4''.8$ distant (SDSS J081804.11+041807.9). After we reported a preliminary list of transients to the Ligo-Virgo EM follow-up GCN circulation list, a spectrum of PS15ccx was taken with the Liverpool Telescope by Steele, Copperwheat & Piascik (2015). They report it as a SN Ia at age 15-23 days post maximum at a redshift $z \simeq 0.097$.

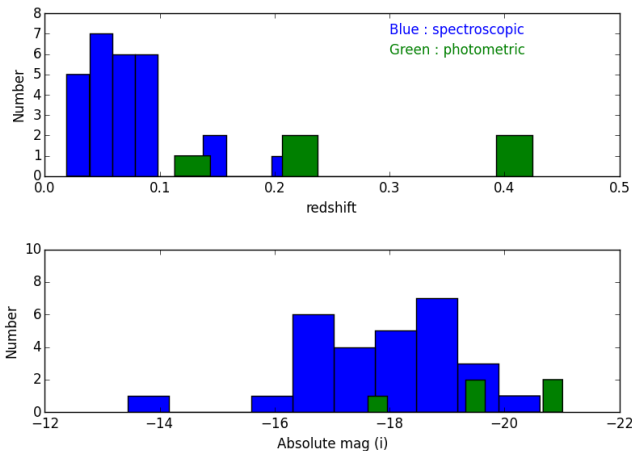


Figure 5. Histograms of the redshift distribution and absolute magnitudes ($M_{i_{P1}}$) of the confirmed SN or likely SN transients. The objects in blue either have a spectroscopic redshift from the transient itself, or host galaxy. The objects in green have a photometric redshift of the host galaxy from SDSS DR12. The AGN/QSO candidates are not included. All magnitudes are in i_{P1} apart from one (PS15ckf) which is in z_{P1} .

4.2 Transients with no spectroscopic classification

For those transients that do not have spectroscopic data, we have assessed their nature from their proximity to host galaxies and the spectroscopic, or photometric redshifts of those hosts. This allows an estimate of the absolute magnitude of the transient, which is the absolute magnitude of the brightest Pan-STARRS1 point in the lightcurve. In doing this, foreground extinctions from Schlafly & Finkbeiner (2011) are applied. Where the association with a host galaxy is likely (where the transient is within a projected distance of 30 kpc), this is then a lower limit to the absolute peak magnitude since the transient may have been brighter before PS1 discovery and internal host galaxy reddening may apply. However it serves to illustrate which transients are consistent with the standard, known supernova population. In addition to the 19 spectroscopically classified transients, and 4 spectroscopically known AGN/QSOs, a further 9 of the 43 were associated with galaxies with host redshifts. There are 3 objects which are either known CVs or likely QSO/stellar variables. Which leaves 21 objects with no confirmed spectroscopic redshifts (of these, 5 have photometric redshifts). These 21 objects are discussed in the following subsections and we outline the most probable nature.

4.2.1 PS15ccw

The redshift of the closest galaxy (SDSS J085730.63+043202.3) is $z = 0.072$ from SDSS DR12. PS15ccw is $6''.2$ from the galaxy core which is a projected physical distance of 8.2 kpc. At this distance the absolute magnitude of the brightest PS1 point is $M_i = -18.2$. We collected a lightcurve covering about 30 days in gri_{P1} , and Fig. 6 compares lightcurves of typical supernovae. The three SN template lightcurves are an i -band lightcurve of SN2005gb (type Ia, $z = 0.09$) from the Sloan Digital

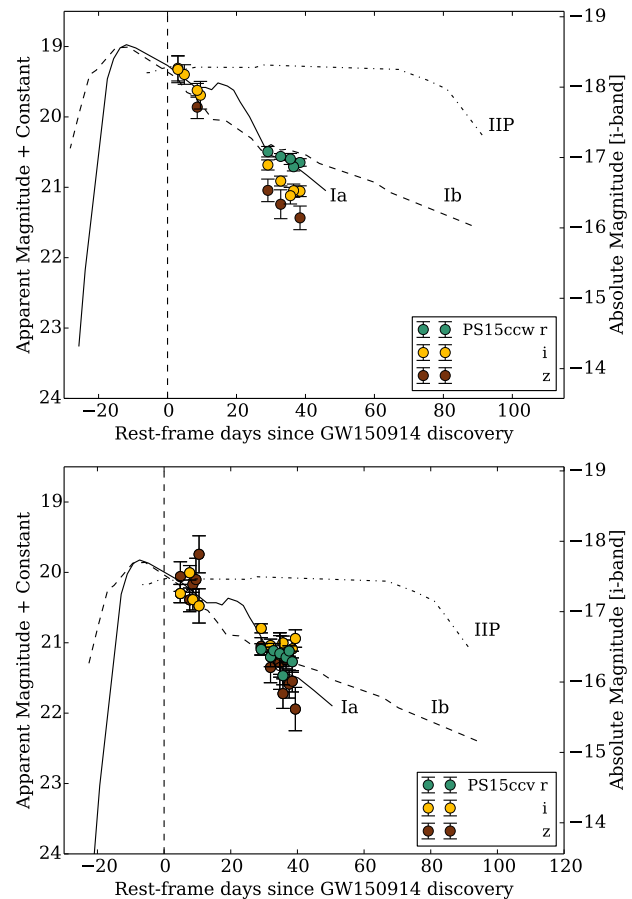


Figure 6. Comparison of the measured lightcurve of PS15ccw and PS15ccv in the riz_{P1} filters with three typical SNe at similar redshifts observed in the same filter systems.

Sky Survey-II Supernova (SN) survey (Holtzman et al. 2008) and two from the Pan-STARRS1 Medium Deep Survey. PS1-12bmp is a type II-P from the sample of Sanders et al. (2015) and the i_{P1} lightcurve is shown here ($z = 0.063$). PS1-13avb is a type Ib (Wright et al. 2015) at $z = 0.0705$ and again the i_{P1} lightcurve is shown. Each lightcurve has been scaled (arbitrarily) to the same peak magnitude of 18.8, but no k -corrections have been applied since all the SNe are at similar redshifts. The time axis has been corrected for time dilation for each and is in the restframe. This straightforward comparison indicates that the location, lightcurve and absolute magnitude of the transient is compatible with it being a supernova in this galaxy and likely either a type Ia or type Ib/c. It is mostly likely a type Ia, since its peak absolute magnitude would be quite bright for a type Ib/c.

4.2.2 PS15ccv

This transient is located very close to the core (within $0''.6$) of a spiral galaxy with a spectroscopic redshift of $z = 0.071$ (SDSS J085523.02+044118.7), or a projected distance of 0.8 kpc. The absolute magnitude of the brightest PS1 point is $M_i = -17.9$. The transient is detected with a declining lightcurve in $r_{P1}i_{P1}z_{P1}$ over a period of 30 days. Similar to PS15ccw, a comparison to the same type Ia, Ib and II SNe in

the same filters shows the lightcurve to be compatible with a SN of type Ia or type Ibc. Again, the location, lightcurve and absolute magnitude of the transient is compatible with it being a supernova in this galaxy and likely either a type Ia or type Ibc. Almost certainly this implies that we discovered PS15ccw and PS15ccv 20-30 days after explosion, during their decline phase and hence they exploded 10-20 days before the GW detection. Another possibility is that they are both very old type II-P SNe which fall off the plateau between the first and second group of points. Either way, we rule these out as related to GW150914.

4.2.3 QSO variability : PS15ckh, PS15ckk, PS15cek and PS15dfz

PS15ckh is the known QSO SDSS J092455.87+021924.9 which was studied in detail by Inada et al. (2003) and shown to be a multiply lensed QSO. The high resolution images presented in Inada et al. (2003) resolve the source into 5 separate components, two of which are confirmed as the lensed QSO at a redshift of $z = 1.524$. In the epoch of the brightest flux excess (on MJD=57310.61218), we measure $i_{P1}=19.2$ in the difference image at the position of component A (which Inada et al. measured at $i = 18.87$). We clearly resolve additional flux excess at a position $1''9$, directly south, at the position of component B of Inada et al. (2003). This indicates that both A and B have flux excesses in these epochs at approximately the same ratio as measured in Inada et al. (2003). We do not detect a flux excess from component C in the difference images. Further analysis is warranted, but outside the scope of this paper.

PS15ckk is detected as a bright transient in i_{P1} , z_{P1} , $y_{P1} \sim 16 - 16.4$ in the difference images. However this is the known, catalogued variable AGN NPM1G-09.0361 in Véron-Cetty & Véron (2001). PS15cek is a known low redshift galaxy with an active nucleus also identified in Véron-Cetty & Véron (2001) and known as 2MFGC 07447 (amongst other names) in NED. The flux excess measured for PS15cek is $i_{P1} \simeq 17$ over 25 days. PS15dfz is the known object SDSS J095459.62+041408.3 which is a QSO at $z = 0.844$ (with $i = 19.28$) and is detected with a flux excess of $i_{P1} = 20.65 \pm 0.05$ on two epochs.

4.2.4 PS15cvz

This object is $3''4$ from the galaxy SDSS J100541.42+010530.0, which has a spectroscopic redshift of $z = 0.069$ and is therefore 4.3kpc in projection. It was discovered at $i_{P1} = 19.6$ and detected twice on separate nights by PS1, the first being 2015 October 13 some 29 days after GW150914. It is also visible in a SNIFS image taken on 2015 October 28. The absolute magnitude of this first point is $M_i = -17.8$, and hence is compatible with being a supernova in this galaxy.

4.2.5 PS15cwm

This is detected 5 times over a period of 10 days beginning on 57310.60, or 31 days after GW150914. The brightest magnitude reported is $i_{P1} = 20.9$ and there is a series of non-detections stretching to about 20 days before the first

PS1 point. There is a galaxy with an early type spectrum at $z = 0.224$ (SDSS J093001.39+065800.0) which is $13''8$ south east of the transient. This corresponds to a distance of 48kpc, which is somewhat too large to be confident of association. A closer, but fainter galaxy ($i = 18.7$; SDSS J093001.16+065819.8) is $7''4$ distant (or 26kpc) and has a photometric redshift of $z = 0.26 \pm 0.03$. A redshift of $z = 0.22 \pm 0.07$ implies $M_i = -19.1_{+0.9}^{-0.7}$, which is within the plausible ranges of normal supernovae. It is likely that the transient is associated with one of these galaxies, or with an undetected dwarf at a similar redshift. The lightcurve evolution is compatible with a supernova.

4.2.6 PS15cvv

This transient is detected multiple times in filter i_{P1} between 57310.61 and 57320.62 with a fairly flat evolution at $i_{P1}=20.20 \pm 0.06$. There is no host galaxy or star within 10 arcsec in either the PS1 3π reference stack or SDSS DR12. A number of faint galaxies ($r \simeq 21 - 22$) are clustered around the transient at distances of 12 - 18 arcseconds and with uncertain photometric redshifts of 0.3 - 0.7. It is likely this is a foreground supernova, and as it was detected first on 57310.61, or 31 days after GW150914 (with non-detections on 57297.63) we have no evidence for it being a slowly rising transient.

4.2.7 PS15cvx

The transient is $2''3$ from the centre of the likely host galaxy 2dFGRS N152Z175 with a spectroscopic redshift of $z = 0.152$. It was detected multiple times over 10 days beginning MJD=57308 and with a peak magnitude of $i_{P1}=20.1$, it corresponds to $M_i = -19.2$. We have no evidence in the lightcurve for it being a slowly rising transient so its discovery date makes it incompatible with the time of GW150914.

4.2.8 PS15cwa

The transient is $3''9$ from an obvious galaxy in the PS1 images, and also catalogued as the UV source GALEXASC J101318.70-105447.8. No redshift information is available for either the host or the transient. It was detected starting 57310.62, or 31 days after GW150914 and faded slowly (0.6 mag) over 10 days. With the data available, this appears to be a normal supernova.

4.2.9 PS15cwk

The transient is $15''4$ from the core of the 2MASS extended source 2MASX J10135545-1252341 which is a resolved SO/Sa galaxy in the PS1 multi-colour images and has a diameter of approximately $18''0$. It was detected starting 57310.63, or 31 days after GW150914 and remained flat for 10 days. With the data available, this appears to be a normal supernova.

4.2.10 PS15cvw

PS15cvw is coincident with a $r = 22.7$ object which SDSS DR12 classifies as a star. The star galaxy separation is not

trustworthy at these flux levels and this is likely a faint host galaxy. Multiple detections beginning 57313.61, for 8 days indicate a slowly fading object that is compatible with being a supernova.

4.2.11 PS15cmp

This is only detected on one night (MJD=57314.6) but in all three filters that were taken ($r_{P1}i_{P1}z_{P1}$ images) at $i_{P1}=21.68$. It is not close to any catalogued source and the nearest galaxy is SDSS J085423.78+035330.1 which is $31''.5$ from the transient and at $z = 0.097$, this would be 55 kpc. That is quite a large distance, although not unprecedented for SNe. We checked the minor planet centre to see if it was a slow moving, known minor planet. The nearest object is 2016 AH73 ($V = 22.5$), but at 2.7 arcmin away it is unlikely to be the same object. It is likely that this is a faint SN that has crept above the detection limit on one night and remained below on the other images.

4.2.12 PS15crh

PS15crh is coincident with a $r = 21.9$ object which SDSS DR12 classifies as a star. The star galaxy separation is not trustworthy at these flux levels and this is likely a faint host galaxy and supernova. The transient was discovered on MJD=57314.58 (35 days after GW150914) at $r_{P1}=21.39$, and detected at similar mags 5 days later (and also 50 days later in normal PSST operations). The lightcurve data are compatible with it being a flat type II-P supernova.

4.2.13 PS15cwh

This faint transient is $13''.5$ from the centre of the likely host galaxy SDSS J085414.34+030504.0 with a spectroscopic redshift of $z = 0.028$. It was detected at $i_{P1} = 21.96 \pm 0.07$, between 57282.6 and 57314.59 and hence would appear to be a long lived faint transient (with $M_i \simeq -13.4$), 7.5 kpc from the centre of the host which was detected three days after the GW150914. However in previous imaging of this field on 57181.26 by PSST (Huber et al. 2015a,b) we detected a source at $z_{P1} = 18.83 \pm 0.07$ and hence this is likely to be a very old SN which was $M_z = -16.6$ at 100 days before GW150914 which is now in the tail phase. A bright stellar outburst in the host (Pastorello et al. 2010, e.g. an LBV type giant outburst) is possible, although $M_z = -16.6$ would be quite luminous for such a transient, or a foreground variable. With this historical detection, we rule out that this is an intrinsically faint transient which occurred within 3 days of GW150914.

4.2.14 PS15cri

No host at all, but multiple detections in the i_{P1} filter on 4 separate nights. This is likely a hostless supernova,⁵

⁵ By hostless, we mean that either the host is too faint to be detected in our reference stacks or the SN has host galaxy which is quite far from the SN position and at a redshift that is difficult to spatially associate it.

4.2.15 PS15cwe

No host detection at all, but multiple detections on 4 separate nights in the i_{P1} and z_{P1} filters, Again it is likely a hostless supernova.

4.2.16 PS15crk

The transient is $6''.5$ from an resolved galaxy in the PS1 images and the galaxy is catalogued as the UV source GALEX-ASC J103003.03-173138.7. With two detections on two separate nights it is likely a SN in this host.

4.2.17 PS15cwg

The transient is $0''.7$ from the core of a resolved galaxy in the PS1 images, and this galaxy is also catalogued as the 2MASS extended source 2MASX J10191950-0916015. With two detections on two separate nights it is likely a SN in this host.

4.2.18 PS15crj

The transient is $1''.9$ from a resolved galaxy in the PS1 images, and also catalogued as SDSS J094242.07+021811.1 with a photometric redshift of $z = 0.41 \pm 0.09$. This is a likely supernova, but the photometric redshift is probably an overestimate of the true redshift (see Section 6 for a discussion on the use of photometric redshifts)

4.2.19 PS15cwc

This is a faint transient with multiple detections on 2 separate nights. It is coincident with a faint, but clearly detected extended source in the PS1 i_{P1} stacks. With two detections on two separate nights it is likely a SN in this faint host.

4.2.20 PS15cqx

The transient is $2''.9$ from the centre of the likely host galaxy 2MASX J10050385-0629439 with a spectroscopic redshift of $z = 0.054481$. This is close to the bright core of the host galaxy, but it is detected on at least 3 separate nights and appears real. With only foreground extinction applied it has $M_i = -16.6$, but could suffer from more extinction from within the host. It is consistent with being a SN.

4.2.21 PS15cqw

This is a $2''.0$ from a resolved galaxy in the PS1 images, and which is also catalogued as $r = 19.3$ source SDSS J094506.56+011702. The transient is one the fainter detections at $i_{P1}=21.99$, but is detected on three separate nights. The host has a photometric redshift of $z = 0.22 \pm 0.03$ in SDSS DR12. The object is consistent with being a SN.

4.2.22 PS15cwd

Transient is detected in multiple nights and is $5''.5$ from a resolved galaxy in the PS1 images, and also catalogued as UV source GALEXASC J100806.68-142514.1. The object is consistent with being a SN.

4.2.23 PS15dgd

This transient is offset by $5''.6$ from the core of the host 2MASX J10272567-1458190. It has no redshift information available. Detected on 3 separate nights, the object is consistent with being a SN.

4.2.24 PS15dgc

This is in the host galaxy 2MASX J10182042-1031244 0.11 (offset by $6''.6$ from the core) with a spectroscopic redshift of $z = 0.055749$. Detected on four nights at $i_{P1}=20.4$, it has an absolute magnitude of $M_i = -16.6$, and is consistent with being a SN.

4.2.25 PS15dgb

Offset from a resolved host galaxy in PS1 (uncatalogued to date and the PS1 survey name is PSO J151.1810-15.0013) with no redshift information. Detected on 4 nights, it is consistent with being a SN.

4.2.26 PS15dga

This is $2''.2$ from the core of the host galaxy 2MASX J10044252-0931139 0.037 with no redshift information. Detected on 4 nights, it is consistent with being a SN.

4.2.27 PS15dfy

This object is coincident with a faint host galaxy SDSS J095248.77+063804.2 at $r = 21.45 \pm 0.08$ and has a photometric redshift of $z = 0.582 \pm 0.123$. It has also been recorded as a transient by CRTS and is known as CSS141127-095249+063804 and MLS130216-095249+063804 at varying magnitudes between 19.5-20 (e.g. Drake et al. 2013). It is likely a variable QSO.

4.2.28 PS15dfx

Offset from clear host galaxy (uncatalogued to date) detected in the PS1 image stack (object called PSO J147.7171-4.1633 in the PS1 3π survey).

4.2.29 PS15dfw

This is $0''.89$ from the galaxy SDSS J094411.68+045452.8 with $r = 20.42 \pm 0.09$ and a photometric redshift $z = 0.113 \pm 0.0814$. It is also detected some 45 days later in routine operations of PSST, at $w_{P1}=22.1$. It is consistent with being a SN.

4.2.30 PS15dfv

This is within $1''.0$ from SDSS J094138.31-021021.7 at $r = 20.18$ which is morphologically classified as a star. It is listed in the MilliQuas catalogue as a QSO at $z = 2.1$, hence this is likely QSO variability.

4.2.31 PS15dfu

Offset from the galaxy SDSS J093424.45+064800.4 by $2''.7$, which has a spectroscopic redshift go $z = 0.0866$.

4.2.32 PS15dft

Coincident with the faint SDSS star $r = 20.5$, and this is already known CV candidate ASASSN-15se (for details of ASAS-SN see Shappee et al. 2014)⁶.

4.2.33 PS15dfs

Coincident with SDSS J092137.60+120138.0 red galaxy, at $r = 20.27$ and which has a photometric redshift of $z = 0.424 \pm 0.079$

4.2.34 PS15dfr

Coincident with SDSS J091829.05+114010.6 ($r = 22.29 \pm 0.14$) and which has a photometric redshift of $z = 0.549 \pm 0.117$. It is also the recurrent transient MLS140206-091829+114011 and possibly a stellar variable or a variable QSO.

5 QUANTIFYING THE SENSITIVITY OF THE SEARCH

The histogram of measured redshifts is shown in Fig 5. This includes all transients with either a spectroscopic redshift of the transient, or the host galaxy, or a photometric redshift of the candidate host. There are five photometric redshifts included for comparison. The histogram of peak absolute magnitudes (all in i_{P1} , apart from PS15ckf which is in z_{P1}) is also shown in Fig 5. This illustrates that our transient discoveries broadly sample the redshift regime $0.05 \lesssim z \lesssim 0.15$, with absolute peak magnitudes $-19 \lesssim M_{i_{P1}} \lesssim -16$. The latter are normal supernova magnitudes which illustrates that if an EM counterpart for GW150914 were to be accessible in our imaging it would need to reach supernova-like luminosities. If we assume that none of the detected transients are associated with GW150914, then it is useful to set some upper limits to our search.

5.1 Verifying the search efficiency by comparisons to SN rates

To estimate the number of SNe that we expect to detect in our search we performed a simple survey simulation. In the simulation we input:

⁶ <http://www.astronomy.ohio-state.edu/~assassin/transients.html>

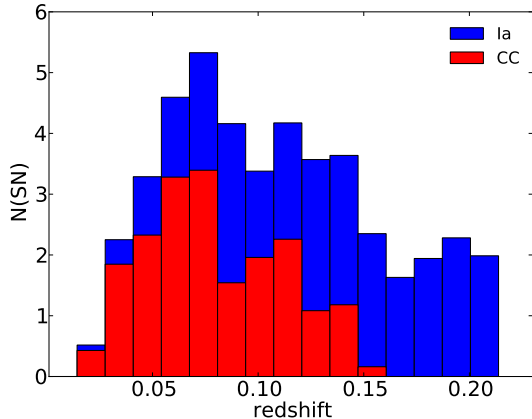


Figure 7. Simulated numbers of core-collapse and type Ia SNe predicted to be detected within the sky survey area and their redshift distribution. See Section 5.1 for details.

- the survey area, the time distribution of the observations, the detection efficiencies at the different epochs. The latter are shown in Fig. 9
- the light curves of template SNe are used to predict the observed light curves at different redshifts. For the computation we use the distance modulus derived from the redshift adopting standard cosmology and we include k -corrections for any given filter (as in Cappellaro et al. 2015)
- the rate per unit volume of the different types of SNe. As reference we use the local rate measurements of Li et al. (2011) and the average rate evolution from the recent compilation of Cappellaro et al. (2015)

The observed light curves along with the survey observing log allowed us to derive the control times for the different SN types for each considered redshift bins. The survey area and standard cosmology define the survey volume for each redshift bin. The expected number of SNe at each redshift is obtained simply by multiplying the SN rate by the control time and the survey volume and is shown in Fig. 7. From this computation we predict a total number of 50 SNe of which 60 per cent should be of type Ia. If we limit to a redshift $z < 0.1$ we expect 22 events with an equal number of type Ia and core collapse. Considering the uncertainty in SN rates and the sampling statistics the number of detected SNe and their redshift distribution is quite consistent with our predictions from measured cosmic SN rates.

To corroborate this with a simple calculation, the number of SNe within the volume defined by $z < 0.1$ and our sky survey area can be predicted. The volumetric rates of type Ia SNe within $z \lesssim 0.15$ have been estimated as $2.9 \pm 0.6 \times 10^{-5} \text{ Mpc}^{-3} \text{ yr}^{-1}$ (converted to $H_0 = 72$, which we use here) by Dilday et al. (2010) and $2.5 \pm 0.5 \times 10^{-5} \text{ Mpc}^{-3} \text{ yr}^{-1}$ by Botticella et al. (2008). Similarly the summary of Horiuchi et al. (2011) of the low redshift core-collapse SN surveys of Cappellaro, Evans & Turatto (1999); Botticella et al. (2008); Li et al. (2011) suggests a volumetric rate at $z \lesssim 0.1$ of $10 \pm 3 \times 10^{-5} \text{ Mpc}^{-3} \text{ yr}^{-1}$ for core collapse (types II and Ibc). The number of type Ia SNe that these rates predict within the 440 square degrees, is the volumetric rate multiplied by the control time (CT), where CT is the time spent

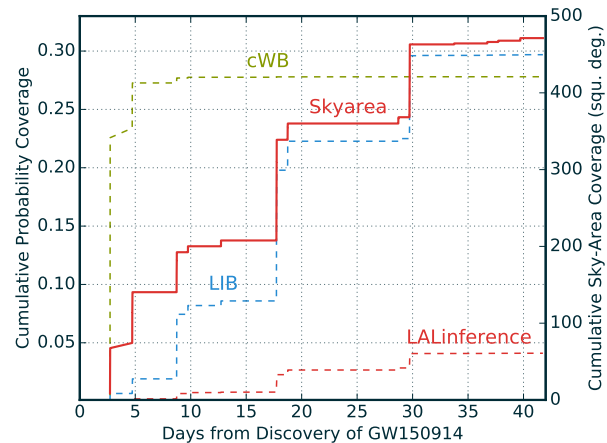


Figure 8. Cumulative sky coverage mapped by Pan-STARRS1 as function of time since the GW150914 trigger is shown in solid red line. The cumulative probability of the LIGO sky maps covered are shown as broken lines which each referring to the particular sky probability map released by LIGO. The first two maps released early where the cWB and LIB, while the LALInference map was the most authoritative.

by each SN in a detectable magnitude range. For a type Ia SN at $z \simeq 0.1$, the peak magnitude would be in the range $i_{P1} = 19.5_{-0.5}^{+0.3}$, and therefore it would be detectable above the $i_{P1}=21$ limiting magnitude of Figure 9 if it exploded within the previous 50 ± 15 days. Therefore the later deeper limits (which cover the whole 440 square degree region) effectively encompass the earlier, shallower limits over a smaller portion of the field. With this control time of 45 ± 15 days, the expected number of type Ia SNe in this volume defined by $z \lesssim 0.1$ is

$$n = V_{z < 0.1} \frac{A_{\text{PS1}}}{41253} \frac{45 \pm 15}{365} (2.9 \pm 0.6 \times 10^{-5}) \quad (3)$$

With a co-moving volume of $V_{z < 0.1} = 0.3 \text{ Gpc}^3$ (for $H_0 = 72$, $\Omega_M = 0.3$ and $\Omega_\Lambda = 0.7$), and a survey area of $A_{\text{PS1}} = 440$ square degrees, we should detect approximately 12_{-5}^{+8} type Ia in the PS1 footprints. We find 9 spectroscopically confirmed type Ia SNe within this redshift range, 8 spectroscopically confirmed type II or Ibc and 8 candidate SNe in galaxies with redshifts less than $z = 0.1$. If these unconfirmed 8 are roughly split in equal proportions as the spectroscopically confirmed sample, then we are likely to have discovered a sample of approximately 13 type Ia SNe. The unconfirmed sample (in galaxies with no host redshift) are likely to be at higher redshift than $z \sim 0.1$. Hence our recovered SN population is in good agreement to the expectations from the type Ia volumetric rates.

5.2 Interpreting the sensitivity limits in the context of GW150914

Our joint Pan-STARRS and PESSTO search cannot set significant and complete upper limits to the magnitude of any optical counterpart because we could not map out the southern sky localisation region. Furthermore, the obvious complication is illustrated in Figure 1, which shows that the northern sky localisation region was not mapped out uniformly

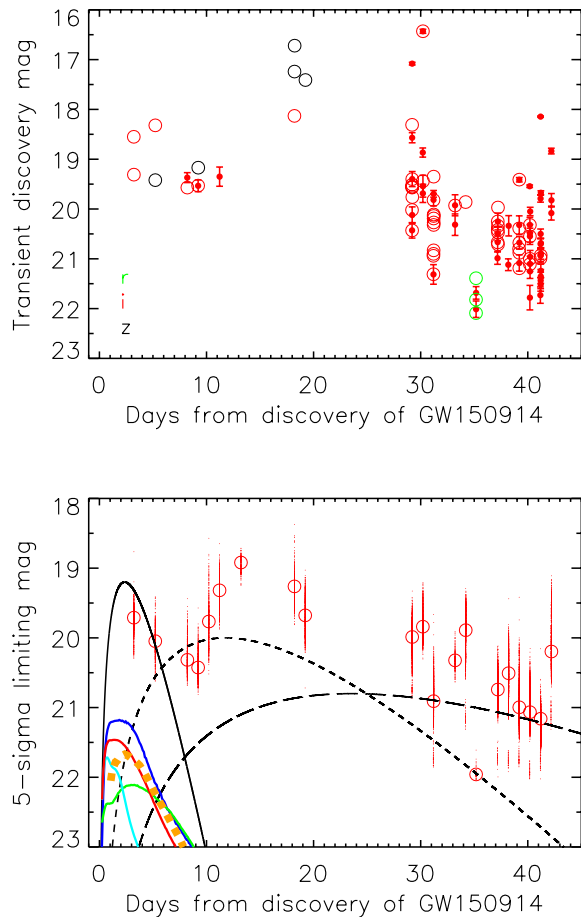


Figure 9. Top Panel : The magnitudes of transients discovered as a function of time from the discovery of GW150914. The solid red circles are the faintest i_{P1} magnitude measured for each of the 56 transients. The open circles are the discovery magnitudes for each transient in the filter they were first detected (green is r_{P1} , red is i_{P1} and black is z_{P1}). **Bottom panel:** The 5σ detection limits for all i_{P1} images determined from fake source injection and recovery. Each individual GPC1 skycell is plotted as a point (there are approximately 51 skycells per PS1 pointing) with the median value on each night denoted by the open circles. The simulated lightcurves of three transients with parameterised lightcurves and characteristic timescales as defined the text of 4d, 20d and 40d which have been scaled in flux to be detectable at signal levels similar to those for measured objects. The four coloured lightcurves (solid lines) in the bottom right are the model lightcurves for compact mergers from Kasen et al. (2015) and Barnes & Kasen (2013). The orange dashed curve is the brightest BH-NS merger model of Tanaka et al. (2014; model MS1Q3a75.k1.AB). The models and are discussed in the text in Section 5.2.

in time. Ideally we would have surveyed the whole northern region within 24hrs from the time of trigger and repeated it to give a flatter temporal distribution in our sensitivities. However as explained in Section 3 this was not possible due to the Right Ascension range of the region. In addition, the sensitivity of the Pan-STARRS imaging of the error region is highly non-uniform. As discussed in Section 3, the PS1 telescope could only reach the north western area of the GW150914 probability map during the first 3-10 days after

the discovery and these fields were observed at typical airmasses of $1.8 \lesssim \sec z \lesssim 2.8$ and close to 18 degree twilight.

The time sequence of mapping out the error region is shown in Figure 1 and in Figure 8. The consequence of the field rising to accessible altitudes to allow longer observing sequences (in darker skies) is illustrated in Figure 9. These two panels illustrate the depths of the fields we reached, through the direct measurement of faint objects and calculations of the 5σ limiting magnitudes. We plot the i_{P1} discovery magnitudes of each of the 56 transients in the $r_{P1}i_{P1}z_{P1}$ filters and the faintest magnitudes recorded. Then we show the estimated 5σ limiting magnitude in each Pan-STARRS skycell. The 60 Pan-STARRS chips are processed individually and warped onto sky coordinates in predefined skycells (approximately 51 per pointing). For each of these, we calculate the nominal 5σ limiting magnitude from photon statistics of the sky background and read noise. A number of fake stars (typically 500) are then inserted into each of the skycells at magnitudes around the nominal value and the 50 per cent recovery efficiency is measured (where an object must have a significance of 5σ to be recovered). This is adopted as the 5σ limiting magnitude. This quantifies the sensitivity of the full system from PS1 imaging through difference imaging, object detection and filtering as discussed in Section 3. The nominal calculation and the 50 per cent efficiency measurements are in good quantitative agreement. The fake stars are positioned randomly in the images, and are mostly on blank sky. Transients that are coincident with galaxies will typically have higher background contamination noise than our randomly placed sample. This is hard to quantify since it will critically depend on the position within a galaxy, and the surface brightness at that point. Candidates for compact binary mergers (e.g. NS-NS mergers) have been often found to lie well outside galaxies (Berger 2014) and hence the limiting magnitudes we calculate would be appropriate. Nevertheless we caution that for objects inside galaxies, the limiting magnitudes will be lower (as they would for any other imaging survey). It illustrates the sky brightness and high airmass problems affecting the imaging in the first 10 days, then the poor weather on Haleakala in the next 10-15 days. The best observing conditions were between 27 – 45 days after GW150914. During this period we typically reach 5σ detection sensitivities of $i_{P1} = 21.0 \pm 0.5$ in exposures which typically have exposure times 30-80 sec, airmass=1.5-2.7 and image quality of FWHM=1".0 - 1".4.

There are now quantitative models for the lightcurves of merging neutron stars which include heating from radioactive heavy elements and ^{56}Ni combined with realistic opacities from r-processed elements (and ejecta masses), such as those recently calculated by Barnes & Kasen (2013), Kasen, Badnell & Barnes (2013), Kasen, Fernández & Metzger (2015) and Tanaka & Hotokezaka (2013). These have been termed kilonovae, as they are fainter than supernovae and mostly have shorter timescales.

The compact binary that caused GW150914 is estimated to be a pair of binary black holes and not merging neutron stars. However as there are no quantitative predictions for what (if any) optical radiation merging black holes may produce, we show the various quantitative models for merging neutron stars. Even if they are not directly applicable here, they indicate the limits we would need to reach to place meaningful constraints. The models in Figure 7 are

the disc wind outflows of compact object mergers (blue) of Kasen, Fernández & Metzger (2015); the r-process powered merger model which includes a ^{56}Ni -dominated wind (red) of Barnes & Kasen (2013); a merger model with iron-group opacity with $M_{\text{ej}} = 0.01M_{\odot}$ by the same authors (cyan); and a merger model for opacity dominated by r-process elements, with $M_{\text{ej}} = 0.1M_{\odot}$ (green) also by the same authors. We have determined i_{P1} synthetic magnitudes, based on the spectra in these papers and scaled them to the closest plausible distance for GW150914 (190 Mpc). The NS-NS merger models of Tanaka & Hotokezaka (2013) are of similar peak luminosity and timescales and are useful alternatives. In addition, we also show the brightest BH-NS merger models of Tanaka et al. (2014) to illustrate the diversity of theorised objects (also scaled to 190 Mpc). The comparison shows we are not reaching the depth, at this distance to probe these types of merger model. However the depth of our survey fields at 30-40 days did reach these sensitivities and if the field had been better placed in the sky we would have reached these depths. This bodes well for future searches.

Metzger et al. (2015) have further predicted that neutron powered pre-cursors of kilonovae may be detectable, through the decay of free neutrons. These are brighter, bluer and faster than the heavy element radioactive decay from the Kasen, Badnell & Barnes (2013) kilonova models. We do not plot them here, as we are not probing the short timescales predicted by those models (hours to 1-2 days).

For BH-BH mergers, the situation is much less clear and there are no published EM lightcurve predictions that could be quantitatively compared with our data to at least determine how deep one might need to get in the UV/optical/NIR to detect a counterpart (Kamble & Kaplan 2013). Tanaka et al. (2014) have also radioactively powered lightcurves for BH-NS mergers which they suggest could be comparable luminosity (or even higher) to NS-NS merger models. To quantify plausible transients we adopt a simple parameterised lightcurve for which we can vary the timescale and peak flux. We can then use this function to quantify the temporally varying limits we have. We use the following function

$$f(t) = \frac{e^2}{4} f_0 \left(\frac{t}{t_0} \right)^2 e^{-t/t_0} \quad (4)$$

This function peaks at $t = 2t_0$, has a peak value of f_0 , and has a full-width-half-maximum of approximately $\text{FWHM} = 3.38t_0$. Choosing flux values to simulate candidates peaking at AB magnitudes of $i = 19, 19.5$ and 21.0 and values of $t_0 = 1.2, 5.9$ and 11.8d we illustrate the sensitivity of the Pan-STARRS search to transients with these three timescales in Fig 9. The values of t_0 correspond to lightcurves with characteristic timescales of $t_{\text{FWHM}} = 4, 10, 40$ days. The simulated transients are set to explode at $t = 0$ on the discovery epoch of GW150914. The plot shows we would be sensitive to transients with these timescales and peak magnitudes of 4d and $i = 19.2$, 20d and $i = 20.0$, and 40d and $i = 20.8$. If we assume a distance to GW150914 of $D_L = 400 \pm 200$ Mpc (from Abbott et al. 2016b) then the following absolute magnitude limits are inferred

(i) **4d timescale** : with a sensitivity of $i = 19.2$, we should have detected transients with a peak flux of $M_i \lesssim -18.8_{+1.4}^{-0.9}$ during the first five days after GW150914. Unfor-

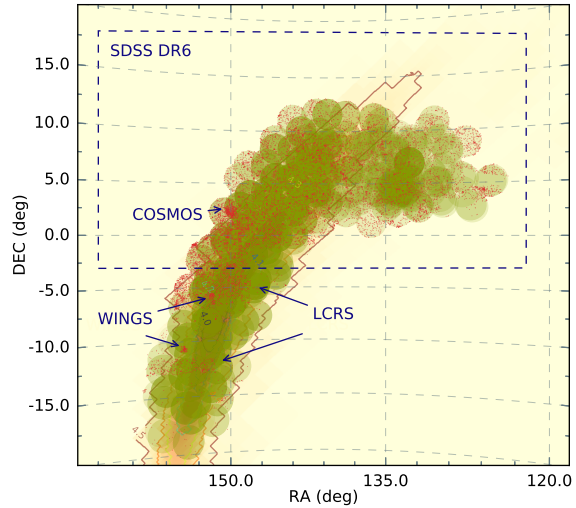


Figure 10. Catalogued galaxies in NED which have a spectroscopic redshift $z \leq 0.15$ and also lie within the PS1 survey area. The green circles are the same as in Fig 1 and show the PS1 pointings. The red dots are all galaxies which have a catalogued spectroscopic redshift that is $z < 0.15$. The sharp drop in the galaxy density below $\delta \simeq -2$ is due to the boundary of the SDSS DR12 survey footprint. The smaller area surveys labelled are described in the text. completeness of galaxy catalogues outside the SDSS footprint.

tunately, due to the RA constraints we were unable to map out the whole northern localisation region, as illustrated in Figure 1. It is quite possible that we missed a transient of this luminosity and timescale simply due to poor coverage in the early days. Future searches will hopefully have more accessible RA ranges to allow this interesting fast timescale to be probed.

(ii) **20d timescale** : with a sensitivity of $i = 20$, we would be sensitive to transients with a peak flux of $M_i \lesssim -18.0_{+1.4}^{-0.9}$ during the first 3 to 17 days after GW150914. Again, as shown in Figure 1, only the northern most region was mapped in any detail up to 17 days and therefore these sensitivity limits again can not be applied over the whole region.

(iii) **40d timescale** : these are the most meaningful limits ($i_{\text{P1}} < 20.8$), since we were able to map the whole skymap region on the timescale of 30-40 days. We would have been sensitive to long lived transients with lightcurves as parameterised above with peak fluxes of $M_i \lesssim -17.2_{+1.4}^{-0.9}$, over the whole 440 square degrees covered (or 4.4 per cent of the probability contours). Although one might expect most electromagnetic sources of GW to be fast decaying (as in the NS-NS and BH-NS mergers), massive asymmetric core-collapse may produce supernovae such as broad lined Ic events (Piro & Thrane 2012). These have similar rise and decay timescales to the 40d parameterised curve and are worth considering even though they are likely to be detectable by LIGO to much smaller distances (up to 50 Mpc).

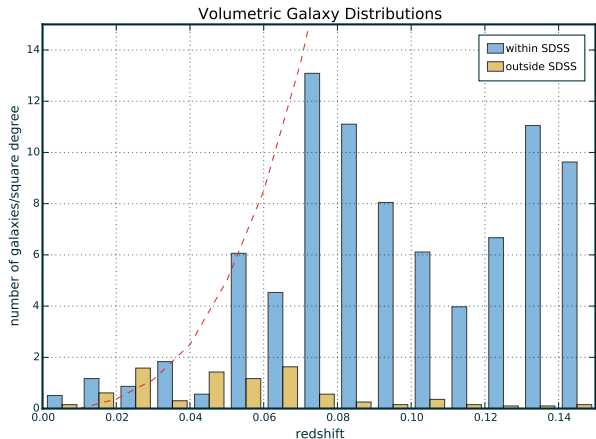


Figure 11. Histogram of galaxy counts per square degree within the SDSS DR12 footprint (blue) and outside SDSS DR12. All galaxies included in this plot have a spectroscopic redshift. The dotted redline plots the volume of the Universe as a function of redshift. It is scaled arbitrarily to approximately match the galaxy counts in SDSS at $0.02 < z < 0.03$, and illustrates that within SDSS the galaxy completeness falls off at ~ 0.07 . Outside SDSS, current catalogues are incomplete beyond $z \sim 0.03$ or about 100 Mpc.

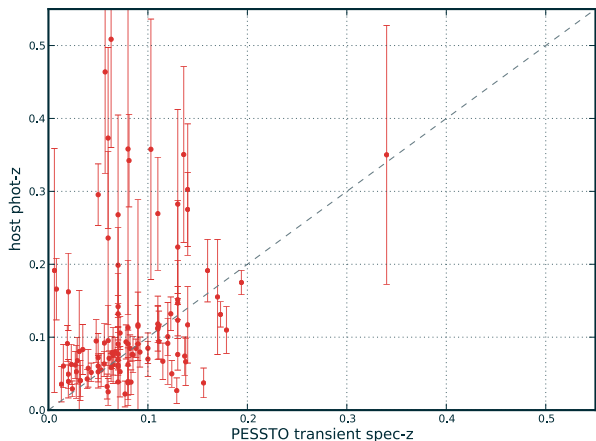


Figure 12. The confirmed spectroscopic redshifts of transients versus the estimated photometric redshift from SDSS DR12. As the spectroscopic catalogues are incomplete, we demonstrate that using the photometric redshifts is not particularly useful to constrain the true redshifts of transients at low redshifts.

6 DISCUSSION

6.1 Our survey in context

Our search of approximately 440 square degrees of the northern sky localisation region of GW150914 over a 41 day period from the discovery yielded 56 reliable astrophysical candidates not including variable stars. This illustrates and quantifies the problem that will be faced in locating the EM counterparts to GW sources in the future. By reaching magnitudes of $i_{P1} = 21 \pm 0.5$, one will find of order 5-10 supernovae per fresh 100 square degrees surveyed within a redshift of $z \lesssim 0.15$, which will be mostly old. This means that any future search for the EM counterparts of GW sources requires significant spectroscopic resources to classify every

transient in the field. It seems clear that there is no easy way to rapidly distinguish candidates and remove the interloping SNe other than spectroscopic confirmation or constraining the luminosities at other wavebands (gamma-ray, x-ray, infra-red or radio). Other early attempts at surveying the error box of GW150914 further illustrate the problem such as the recent work of Soares-Santos et al. (2016); Annis et al. (2016); Kasliwal et al. (2016) and the summary of the broad wavelength range follow-up campaign in Abbott et al. (2016a). The possibilities for the counterpart of GW150914 are as follows, and these could be applied to any counterpart search that returns a null result

- (i) The EM counterpart was outside our survey region. This is probable, given the total probability we covered from the LIGO sky maps is only 4.2 per cent. The original sky map released implied we were covering around 30 per cent with our pointings. In this case there is little we can add, as the southern sky localisation region is significantly favoured.
- (ii) The EM counterpart was in our survey region, but fell below the limits. In this case the sensitivity limits from the model transients with three example timescales set useful targets (in terms of luminosity and timescale) to aim for in future searches
- (iii) The EM counterpart to GW150914 was detected as one of the 56 transients but we don't recognise it as causally linked. This seems unlikely, but it is not ruled out. It maybe that one of the fainter transients discovered in the time window of >24 days after GW150914 is associated and that without a confirming spectrum, or detailed lightcurve no useful discrimination from the SN population is possible. Future surveys of GW localisation regions must still search for known SNe that are rare by volume (or sky area) but are habitually found in the GW regions.

Given the above, the only possibility for improvement (and increasing the probability of detection of a GW counterpart) is to survey the regions rapidly and continuously and be as spectroscopically complete as as possible. A reasonable question then is could survey strategies be adjusted to make use of redshift and flux information of the host galaxy population as suggested by, for example White, Daw & Dhillon (2011) and more recently Gehrels et al. (2015).

6.2 Using galaxy catalogues with spectroscopic and photometric redshifts

The use of galaxy catalogues to pick potential host galaxies within the sky localisation region has the advantage that larger aperture telescopes, with smaller FOV cameras, can focus on these targets and produce significantly deeper images than 0.4-2m telescopes that aim to map the sky region. The bar to this has been the commonly known problem of the incompleteness of galaxy catalogues beyond distances of ~ 100 Mpc ($z \sim 0.025$). Our search provides a useful practical example to investigate if galaxy targeting, from catalogued sources would be useful in the case of GW150914. In Figure 10 we show the known galaxy catalogue within the sky localisation region for GW150914 and the inhomogeneity is immediately obvious. The northern region is dominated by galaxy counts from SDSS and regions of high density are visible as the COSMOS (Scoville et al. 2007) Las Campanas Redshift Survey (LCRS; Shectman et al. 1996) and

Wide-field Nearby Galaxy-cluster Survey (WINGS; Fasano et al. 2006). Such structure has been illustrated by Gehrels et al. (2015) in the ‘‘Census of the Local Universe’’ (CLU) catalogue that they present, which is a union of existing catalogues. The CLU aims to catalogue all galaxies with $L > L_B^*$, where $L_B^* = (1.2 \pm 0.1) \times 10^{10} h^{-2} L_{B,\odot}$ (which corresponds to $M_B^* = -20.5$ for $h = 0.7$). For comparison, the Milky Way galaxy is estimated at $M_B = -20.4$, therefore the CLU is aiming at galaxies with masses larger than the Milky Way within a radius of about 200 Mpc. While Gehrels et al. (2015) show that selecting these high mass galaxies from the union of existing catalogues produces a reasonably encouraging large scale structure pattern (their Figure 1), we illustrate here that for GW150914 such a galaxy targeted strategy would be rather incomplete. This stems mostly from the fact that the distance to GW150914 $z \sim 0.1$ (or 400 Mpc) is much larger than expected for the first LIGO/Virgo bursts up to now ($z \lesssim 0.05$, or 200 Mpc). However even at 200 Mpc, the CLU of Gehrels et al. (2015) drops to below 40 per cent completeness. The severe incompleteness of current galaxy catalogues, with spectroscopic redshifts, is highlighted in our Figure 10 and Figure 11. For this we selected all galaxies within NED with a spectroscopic redshift within the PS1 footprints (Figure 10), then we selected a region within the SDSS DR12 footprint and outside the SDSS area. The number of galaxies (with no luminosity cut-off) per square degree is shown in Figure 11. A simple calculation of co-moving volume is plotted in red, scaled arbitrarily to the galaxy counts at $z \sim 0.02$. This illustrates that the galaxy counts in the SDSS area do not fall off until $z \simeq 0.07$ (300 Mpc). However outside SDSS, the galaxy catalogues are clearly incomplete by some margin beyond $z \simeq 0.03$ (120 Mpc). The conclusion from this is that given the unexpectedly large distance estimate to GW150914, a targeted galaxy search would not have been a viable strategy in this case.

As the Pan-STARRS1 survey will provide a *grizyP1* multi-colour survey of the whole sky above $\delta \simeq -30^\circ$ (Metcalfe et al. 2013, Chambers et al. 2016, in prep) and photometric redshifts of all galaxies (Saglia et al. 2012), we should consider the possibility of using photometric redshifts of transient host galaxies to guide candidate selection. Photometric redshifts of galaxy samples within the range $z < 0.5$ have encouragingly small RMS scatters of typically 2.4 per cent (Saglia et al. 2012). In the second data release (SSDR2), the PESSTO survey (Smartt et al. 2015) produced a catalogue of all transients classified by the survey and the cross-matched host galaxies⁷. This catalogue including the transient object redshift from the PESSTO spectral classifications, the host galaxy spectroscopic redshift (where it existed in NED) and the host galaxy photometric redshift (where it existed in SDSS DR12). This sample of 106 low redshift transients gives a useful sample of transients for which a confirmed spectroscopic redshift exist and a photometric host galaxy redshift estimate can be compared. This is plotted in Figure 12 and illustrates that at low redshift, where GW counterparts are expected to be ($z \lesssim 0.15$), the use of photometric redshift information is of limited value. Around 20 per cent of transients have host photometric red-

shifts that differ by more than a factor 2 from their true value. Perhaps the most useful constraint that could be made is that a selection of host $z_{\text{phot}} \leq 0.15$ (83 objects), produces a pure sample of transients with $z_{\text{spec}} \leq 0.15$. Only 3 objects lie beyond $z_{\text{spec}} > 0.15$, giving a purity of 96 per cent. One might be tempted to use this as a selection for low redshift transients, however the incompleteness (about 20 per cent) caused by the objects with high host z_{phot} values precludes this as a useful selection criteria. It is also dubious whether the z_{phot} selection is actually driving the pure sample of $z_{\text{spec}} \leq 0.15$ objects, since this redshift limit is driven by the limiting magnitudes of the imaging surveys for PESSTO and the sensitivity limit of spectroscopic classification (both around $r \sim 20.5$ for EFOSC2 and the feeder surveys of LSQ, PS1, OGLE etc as described in Smartt et al. 2015). The poor recovery of true redshifts from host z_{phot} illustrates that the relatively high values for 5 of the transients found in the GW150914 region (illustrated in Figure 5 and discussed in Section 4) are likely to be examples of systematic over-estimation as visible in the 20 per cent of significant outliers in Figure 12.

In conclusion, we find that attempting to implement a refined strategy to search for the counterpart of GW150914 (or any GW source at distances greater than ~ 120 Mpc) by using galaxy catalogues would not have been a useful exercise. This targeted galaxy method would certainly be useful at distances below 100 Mpc. However the most plausible skymap and distance information needs to be released early and be reliable for this to be useful and neither occurred for GW150914. If GW sources turn out to have a higher redshift distribution than we expected (e.g. $z > 0.05$, rather than below $z < 0.02$) then the spectroscopic galaxy catalogues currently available are incomplete by large margins (particularly outside the SDSS DR12 footprint). It appears that the most useful strategy is tiling out the entire localisation region and being as spectroscopically complete as possible. Further thought should be given to interpreting the probability maps in a manner that leads to investment of exposure time as a function of sky probability.

6.3 Multi-messenger searches and temporal coincidences

This early multi-messenger search should be seen in context with other wide-field follow-up from high energy triggers with poor sky localisation. Aartsen et al. (2015) triggered a range of wide-field optical facilities to try and identify coincident sources with detections of high energy neutrinos from IceCube. They searched the error circle region of 0.9 square degrees with the PTF, Swift and ROTSE and found one transient, PTF12csy. However searching through archival data from the Pan-STARRS1 3π survey showed that PTF12csy was visible about 158 days before the neutrino detection and unlikely to be causally related. Singer et al. (2015) searched for the optical counterparts to high energy Fermi GRBs, which are detected in the GBM with poor spatial localisation (of the order 10s to 100 square degrees). In this case the PTF camera covered between 30-147 square degrees for 35 separate Fermi GRBs. In each of these cases around ~ 10 optical transients are found that would warrant follow-up. These are mostly SNe or AGN, and Singer et al. (2015) showed that photometric monitoring along with rapid

⁷ Publicly available from <http://www.eso.org/qi/>

spectral typing could uncover the elusive afterglows. A key component to both of these is identifying transients which are both spatially and temporally coincident with the high energy trigger. The work here, searching 440 square degrees (finding 56 transients) goes a step beyond in terms of sky area and contamination by already existing transients.

A key part of removing the contaminating SN population is to use the date and time of the GW source to reject transients which are not temporally coincident. As discussed and illustrated in this paper, a survey of \sim hundreds of square degrees will find mostly old SNe that have exploded in the weeks previously. Effectively we are sampling the history of explosions over a past period which is defined by the length of time they are visible for. A more interesting question is how many new SNe per day per 100 sq degrees are expected to be detected. In Fig. 13 we show these numbers which are calculated from the cosmic SN rates (discussed in Section 5.1). Co-moving volumes were calculated with the cosmology used in this paper to determine the rates, and luminosity distance is plotted to be useable for magnitude estimates. A survey reaching $m = 21$ will typically find 1 new CCSN and 4 new SN Ia per 100 square degrees per 10 days. Which means if we can date the epoch of the explosions with an uncertainty of 10 days, then the numbers in this figure are a reasonable estimate of the rate of contaminating sources. Dating requires a combination of spectra and lightcurves and is generally easier for type Ia SNe than CCNSe since the later show more diversity. This prediction is in reasonable agreement with what we have seen in this search. For $m = 20.5$, we would expect about 12 new SNe in the 440 square degrees in a 10 day window and we find about 6 that (within the uncertainties) are plausibly within the window, plus there are many more candidates for which we have no dates. This does not require that the SNe are found very close to explosion, only that with information around peak that they can be dated. Of course lightcurves which reach closer to the explosion time are very useful to aid dating. For example PTF have demonstrated the science return from discoveries within 24hrs of a deep non-detection (e.g. Cao et al. 2013) and the ATLAS survey (Tonry 2011) will soon be capable of surveying the entire northern sky multiple times per night to $m_{AB} \simeq 20$. For possible GW sources, we expect to be looking for temporal and spatial coincidence of unusual transients, rare types of SNe or those that might be linked to long GRBs (e.g. broad lined Ic SNe) or short GRBs (kilonovae). The early searches may be forced to consider temporal coincidences and the numbers in Fig. 13 serve as a guide. The numbers scale linearly with the uncertainty in the explosion epoch.

7 CONCLUSIONS

For the first detection of GW waves from the LIGO experiment, we have searched for an optical counterpart to the source. We used the sky probability maps provided by LIGO to focus our search on 442 square degrees of sky with the Pan-STARRS1 telescope. We discovered 56 astrophysical transients over a period of 41 days and through a combination of spectra mostly from PESSTO and SNIFS, host galaxy redshifts and photometric monitoring, we quantified

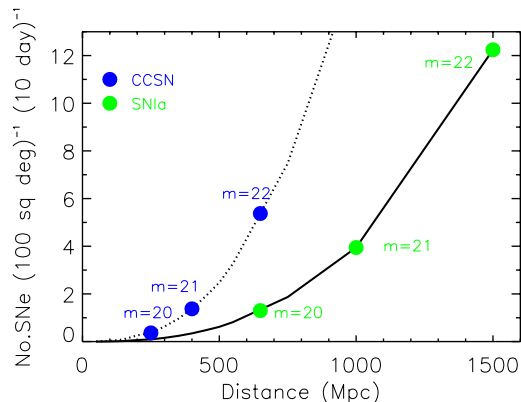


Figure 13. The predicted number of SNe per 100 square degrees per 10 day period, determined from the cosmic SN rates (Section 5.1). The core-collapse rates are the dotted line and the Ia rates are solid line. The solid symbols illustrate the peak magnitude of CCNSe ($M = -17$) and SNIa ($M = -19$) AB mags at the distances, illustrating the numbers expected for difference survey depths. For example, a survey which reaches $m = 22$ can expect to find around 6 CCSN which would have exploded in a 10 day window around the GW.

these objects. All appear to be fairly normal SNe and AGN variability and none is obviously linked to GW150914.

The distance estimated by LIGO to GW150914 of $D_L = 410_{-180}^{+160}$ Mpc, means that relatively faint kilonova type lightcurves would not be detectable by our images which reach $i_{P1} \simeq 20.0$ over the kilonova-like ~ 10 day timescales. The fact that GW150914 is likely to be a BH-BH coalescence means we do not have quantitative models to compare with our limits. We used analytic parameterised lightcurves with different timescales to illustrate the capability of our survey. Had we covered a significant fraction of the probability, we could reach the sensitivity limits of $M_i \leq -17.2_{+1.4}^{-0.9}$ at the distance of GW150914. We treat this early search as a lessons learned exercise and our main findings are :

- Access to the most reliable skymaps as early as possible is key to focusing future searches. The final probability of the most reliable skymap that we covered was 4.2 per cent. This was significantly less than the initial cumulative probability from the first skymap released (which was about 30 per cent). It is critical to invest telescope exposure times on the highest probability regions as early as possible.
- Spectroscopic classification of sources is essential to determine redshift and date the explosion epoch. We provide estimates of the number of contaminating SNe per sky area per 10 days as a guide to the rate of unrelated sources in the GW sky maps.
- We illustrate the capability of the Pan-STARRS1 telescope to survey hundreds of square degrees of sky to AB mags of 19-21.5 rapidly and to produce transients daily. PESSTO is a powerful classification survey that can play an important role in the classification of these optical transients.
- Future searches will benefit from an even quicker response time to map out the sky localisation region within 1 day. We have demonstrated that this is possible in this paper and quantified the contaminating sources arising. The goal

of our, and future surveys will be to map the high probability to region to $m_{AB} \simeq 22 - 23$ mag within 1-2 days.

ACKNOWLEDGMENTS Pan-STARRS is supported by the University of Hawaii and the National Aeronautics and Space Administration's Planetary Defense Office under Grant No. NNX14AM74G. The Pan-STARRS-LIGO effort is in collaboration with the LIGO Consortium and supported by Queen's University Belfast. The Pan-STARRS1 Sky Surveys have been made possible through contributions by the Institute for Astronomy, the University of Hawaii, the Pan-STARRS Project Office, the Max Planck Society and its participating institutes, the Max Planck Institute for Astronomy, Heidelberg and the Max Planck Institute for Extraterrestrial Physics, Garching, The Johns Hopkins University, Durham University, the University of Edinburgh, the Queen's University Belfast, the Harvard-Smithsonian Center for Astrophysics, the Las Cumbres Observatory Global Telescope Network Incorporated, the National Central University of Taiwan, the Space Telescope Science Institute, and the National Aeronautics and Space Administration under Grant No. NNX08AR22G issued through the Planetary Science Division of the NASA Science Mission Directorate, the National Science Foundation Grant No. AST-1238877, the University of Maryland, Eotvos Lorand University (ELTE), and the Los Alamos National Laboratory. This work is based (in part) on observations collected at the European Organisation for Astronomical Research in the Southern Hemisphere, Chile as part of PESSTO, (the Public ESO Spectroscopic Survey for Transient Objects Survey) ESO programs 188.D-3003, 191.D-0935. Some of the data presented herein were obtained at the Palomar Observatory, California Institute of Technology. SJS acknowledges funding from the European Research Council under the European Union's Seventh Framework Programme (FP7/2007-2013)/ERC Grant agreement n° [291222] and STFC grants ST/I001123/1 and ST/L000709/1. MF is supported by the European Union FP7 programme through ERC grant number 320360. KM acknowledges support from the STFC through an Ernest Rutherford Fellowship FOE acknowledges support from FONDECYT through postdoctoral grant 3140326.

This research has made use of the NASA/IPAC Extragalactic Database (NED) which is operated by the Jet Propulsion Laboratory, California Institute of Technology, under contract with the National Aeronautics and Space Administration and data products from the Two Micron All Sky Survey, which is a joint project of the University of Massachusetts and the Infrared Processing and Analysis Center/California Institute of Technology, funded by the National Aeronautics and Space Administration and the National Science Foundation.

REFERENCES

- Aartsen M. G. et al., 2015, *ApJ*, 811, 52
Aasi J. et al., 2014, *ApJS*, 211, 7
Aasi J. et al., 2013, *PRD*, 87, 022002
Abadie J. et al., 2012, *PRD*, 85, 082002
Abadie J. et al., 2010, *Classical and Quantum Gravity*, 27, 173001
Abazajian K. N. et al., 2009, *ApJS*, 182, 543
Abbott B. P. et al., 2016a, *ArXiv e-prints*
Abbott B. P. et al., 2016b, *Physical Review Letters*, 116, 061102
Abbott B. P. et al., 2016c, *ArXiv e-prints*
Acerese F. et al., 2015, *Classical and Quantum Gravity*, 32, 024001
Aldering G. et al., 2006, *ApJ*, 650, 510
Anderson J. P. et al., 2014, *ApJ*, 786, 67
Annis J. et al., 2016, *ApJL*, 823, L34
Bacon R. et al., 2001, *MNRAS*, 326, 23
Baltay C. et al., 2013, *PASP*, 125, 683
Barnes J., Kasen D., 2013, *ApJ*, 775, 18
Berger E., 2014, *ARAA*, 52, 43
Berger E., Fong W., Chornock R., 2013, *ApJL*, 774, L23
Berry C. P. L. et al., 2015, *ApJ*, 804, 114
Blondin S., Tonry J. L., 2007, *ApJ*, 666, 1024
Botticella M. T. et al., 2008, *A&A*, 479, 49
Botticella M. T. et al., 2010, *ApJL*, 717, L52
Brink H., Richards J. W., Poznanski D., Bloom J. S., Rice J., Negahban S., Wainwright M., 2013, *MNRAS*, 435, 1047
Cao Y. et al., 2013, *ApJL*, 775, L7
Cappellaro E. et al., 2015, *A&A*, 584, A62
Cappellaro E., Evans R., Turatto M., 1999, *A&A*, 351, 459
Cenko S. B. et al., 2013, *ApJ*, 769, 130
Chen H.-Y., Holz D. E., 2015, *ArXiv e-prints*
Chornock R. et al., 2014, *ApJ*, 780, 44
Clocchiatti A. et al., 1996, *AJ*, 111, 1286
Cornish N. J., Littenberg T. B., 2015, *Classical and Quantum Gravity*, 32, 135012
Cowperthwaite P. S., Berger E., 2015, *ApJ*, 814, 25
Denneau L. et al., 2013, *PASP*, 125, 357
Dilday B. et al., 2010, *ApJ*, 713, 1026
Drake A. J. et al., 2013, *The Astronomer's Telegram*, 4872, 1
Drake A. J. et al., 2010, *ApJL*, 718, L127
Drout M. R. et al., 2014, *ApJ*, 794, 23
Essick R., Vitale S., Katsavounidis E., Vedovato G., Klimentenko S., 2015, *ApJ*, 800, 81
Fasano G. et al., 2006, *A&A*, 445, 805
Filippenko A. V., 1997, *ARAA*, 35, 309
Finkbeiner D. P. et al., 2015, *ArXiv e-prints*
Flesch E. W., 2015, *PASA*, 32, 10
Fraser M. et al., 2013, *ApJL*, 779, L8
Galbany L. et al., 2016, *AJ*, 151, 33
Gall E. E. E. et al., 2015, *A&A*, 582, A3
Ganeshalingam M., Li W., Filippenko A. V., 2011, *MNRAS*, 416, 2607
Gehrels N., Cannizzo J. K., Kanner J., Kasliwal M. M., Nissanke S., Singer L. P., 2015, *ArXiv e-prints*
Gezari S. et al., 2015, *ApJ*, 804, 28
Goldstein D. A. et al., 2015, *AJ*, 150, 82
González-Gaitán S. et al., 2015, *MNRAS*, 451, 2212
Graham J. F., Schady P., 2015, *ArXiv e-prints*
Guetta D., Della Valle M., 2007, *ApJL*, 657, L73
Hanna C., Mandel I., Vousden W., 2014, *ApJ*, 784, 8
Harutyunyan A. H. et al., 2008, *A&A*, 488, 383
Holtzman J. A. et al., 2008, *AJ*, 136, 2306
Horiuchi S., Beacom J. F., Kochanek C. S., Prieto J. L., Stanek K. Z., Thompson T. A., 2011, *ApJ*, 738, 154
Huber M., Carter Chambers K., Flewelling H., Smartt S. J., Smith K., Wright D., 2015a, *IAU General Assembly*, 22,

- 58303
 Huber M. et al., 2015b, *The Astronomer's Telegram*, 7153, 1
 Inada N. et al., 2003, *AJ*, 126, 666
 Inserra C. et al., 2013a, *A&A*, 555, A142
 Inserra C. et al., 2013b, *ApJ*, 770, 128
 Jin Z.-P., Li X., Cano Z., Covino S., Fan Y.-Z., Wei D.-M., 2015, *ApJL*, 811, L22
 Kaiser N. et al., 2010, in *Society of Photo-Optical Instrumentation Engineers (SPIE) Conference Series*, Vol. 7733, *Society of Photo-Optical Instrumentation Engineers (SPIE) Conference Series*
 Kamble A., Kaplan D. L. A., 2013, *International Journal of Modern Physics D*, 22, 41011
 Kankare E. et al., 2015, *A&A*, 581, L4
 Kasen D., Badnell N. R., Barnes J., 2013, *ApJ*, 774, 25
 Kasen D., Fernández R., Metzger B. D., 2015, *MNRAS*, 450, 1777
 Kasliwal M. M. et al., 2016, *ArXiv e-prints*
 Kasliwal M. M., Nissanke S., 2014, *ApJL*, 789, L5
 Kelly P. L., Kirshner R. P., 2012, *ApJ*, 759, 107
 Klimentenko S. et al., 2016, *PRD*, 93, 042004
 Koppenhoefer J., Afonso C., Saglia R. P., Henning T., 2009, *A&A*, 494, 707
 Lantz B. et al., 2004, in *Society of Photo-Optical Instrumentation Engineers (SPIE) Conference Series*, Vol. 5249, *Optical Design and Engineering*, Mazuray L., Rogers P. J., Wartmann R., eds., pp. 146–155
 Le Guillou L. L. et al., 2015, *The Astronomer's Telegram*, 7102, 1
 Lee C.-H. et al., 2014, *ApJ*, 797, 22
 Li W. et al., 2011, *MNRAS*, 412, 1441
 Lynch R., Vitale S., Essick R., Katsavounidis E., Robinet F., 2015, *ArXiv e-prints*
 Magnier E. A. et al., 2013, *ApJS*, 205, 20
 McCrum M. et al., 2014, *MNRAS*, 437, 656
 McCrum M. et al., 2015, *MNRAS*, 448, 1206
 Metcalfe N. et al., 2013, *MNRAS*, 435, 1825
 Metzger B. D., Bauswein A., Goriely S., Kasen D., 2015, *MNRAS*, 446, 1115
 Metzger B. D., Berger E., 2012, *ApJ*, 746, 48
 Metzger B. D. et al., 2010, *MNRAS*, 406, 2650
 Narayan R., Paczynski B., Piran T., 1992, *ApJL*, 395, L83
 Ngiam J., Chen Z., Bhaskar S. A., Koh P. W., Ng A. Y., 2011, in *Advances in Neural Information Processing Systems 24*, Shawe-Taylor J., Zemel R., Bartlett P., Pereira F., Weinberger K., eds., *Curran Associates, Inc.*, pp. 1125–1133
 Nicholl M. et al., 2013, *Nature*, 502, 346
 Nicholl M. et al., 2015, *MNRAS*, 452, 3869
 Nissanke S., Kasliwal M., Georgieva A., 2013, *ApJ*, 767, 124
 Ofek E. O. et al., 2007, *ApJL*, 659, L13
 Pastorello A. et al., 2010, *MNRAS*, 408, 181
 Phillips M. M., Wells L. A., Suntzeff N. B., Hamuy M., Leibundgut B., Kirshner R. P., Foltz C. B., 1992, *AJ*, 103, 1632
 Piro A. L., Thrane E., 2012, *ApJ*, 761, 63
 Polshaw J. et al., 2015, *A&A*, 580, L15
 Prentice S. J. et al., 2016, *ArXiv e-prints*
 Quimby R. M. et al., 2011, *Nature*, 474, 487
 Quimby R. M., Yuan F., Akerlof C., Wheeler J. C., 2013, *MNRAS*, 431, 912
 Rest A. et al., 2014, *ApJ*, 795, 44
 Rubin A. et al., 2015, *ArXiv e-prints*
 Saglia R. P. et al., 2012, *ApJ*, 746, 128
 Sanders N. E. et al., 2015, *ApJ*, 799, 208
 Schlafly E. F., Finkbeiner D. P., 2011, *ApJ*, 737, 103
 Schlafly E. F. et al., 2012, *ApJ*, 756, 158
 Scoville N. et al., 2007, *ApJS*, 172, 1
 Shappee B. J. et al., 2014, *ApJ*, 788, 48
 Shectman S. A., Landy S. D., Oemler A., Tucker D. L., Lin H., Kirshner R. P., Schechter P. L., 1996, *ApJ*, 470, 172
 Singer L. P. et al., 2015, *ApJ*, 806, 52
 Singer L. P., Price L. R., 2016, *PRD*, 93, 024013
 Singer L. P. et al., 2014, *ApJ*, 795, 105
 Smartt S. J., Eldridge J. J., Crockett R. M., Maund J. R., 2009, *MNRAS*, 395, 1409
 Smartt S. J. et al., 2015, *A&A*, 579, A40
 Smith N., Chornock R., Li W., Ganeshalingam M., Silverman J. M., Foley R. J., Filippenko A. V., Barth A. J., 2008, *ApJ*, 686, 467
 Smith N. et al., 2007, *ApJ*, 666, 1116
 Soares-Santos M. et al., 2016, *ApJL*, 823, L33
 Steele I. S., Copperwheat C., Piascik A., 2015, *GRB Coordinates Network*, 18371
 Taddia F. et al., 2015, *A&A*, 574, A60
 Tanaka M., Hotokezaka K., 2013, *ApJ*, 775, 113
 Tanaka M., Hotokezaka K., Kyutoku K., Wanajo S., Kiuchi K., Sekiguchi Y., Shibata M., 2014, *ApJ*, 780, 31
 Tanvir N. R., Levan A. J., Fruchter A. S., Hjorth J., Hounsell R. A., Wiersema K., Tunnicliffe R. L., 2013, *Nature*, 500, 547
 The LIGO Scientific Collaboration et al., 2015, *Classical and Quantum Gravity*, 32, 074001
 The LIGO Scientific Collaboration, The Virgo Collaboration, 2012, *ArXiv e-prints*
 The LIGO Scientific Collaboration, the Virgo Collaboration, 2015, *GRB Coordinates Network*, 18858
 The LIGO Scientific Collaboration, the Virgo Collaboration, 2016, *ArXiv e-prints*
 The LIGO Scientific Collaboration, the Virgo Collaborations, 2015, *GRB Coordinates Network*, 18330
 Tonry J. L., 2011, *PASP*, 123, 58
 Tonry J. L. et al., 2012a, *ApJ*, 745, 42
 Tonry J. L. et al., 2012b, *ApJ*, 750, 99
 Utrobin V. P., Chugai N. N., Botticella M. T., 2010, *ApJL*, 723, L89
 Valenti S. et al., 2011, *MNRAS*, 416, 3138
 Veres P. et al., 2015, *Icarus*, 261, 34
 Véron-Cetty M.-P., Véron P., 2001, *A&A*, 374, 92
 White D. J., Daw E. J., Dhillon V. S., 2011, *Classical and Quantum Gravity*, 28, 085016
 Woosley S. E., Bloom J. S., 2006, *ARAA*, 44, 507
 Wright D., 2015, *PhD thesis*, Department of Physics and Astronomy, Queen's University Belfast.
 Wright D. E. et al., 2015, *MNRAS*, 449, 451
 Yang B. et al., 2015, *Nature Communications*, 6, 7323

**APPENDIX A: DETAILS OF PAN-STARSS1
FIELDS**

Table A gives a summary of the Pan-STARRS1 observations. Table A2 gives the RA of the proximity to twilight for each filter used to survey the sky probability maps. This lists the maximum RA accessible in each filter for the date given when the sub is 16 degrees below the horizon (for $g_{P1}r_{P1}i_{P1}$), 14 degrees below (for z_{P1}) and 10 degrees below (for y_{P1}). This is indicated in the plots in Figure 1 as vertical lines for the i_{P1} filter.

Table A1. Summary of Pan-STARRS1 observations

Date	MJD	Filters	Exposure Times (sec)	Number of PS1 Exposures
20150917	57282	$i_{P1}z_{P1}y_{P1}$	45,60	34
20150919	57284	$i_{P1}z_{P1}y_{P1}$	20,23,35	59
20150922	57287	$i_{P1}z_{P1}y_{P1}$	40,45,68	45
20150923	57288	$i_{P1}z_{P1}y_{P1}$	25,30,37	49
20150924	57289	$i_{P1}z_{P1}y_{P1}$	30,45	45
20150925	57290	$i_{P1}z_{P1}y_{P1}$	30,45	44
20150927	57292	i_{P1}	35	4
20151002	57297	$i_{P1}z_{P1}y_{P1}$	25,35	57
20151003	57298	$i_{P1}z_{P1}y_{P1}$	25,40	65
20151013	57308	$i_{P1}z_{P1}y_{P1}$	25,35	88
20151014	57309	$i_{P1}z_{P1}y_{P1}$	30,60	77
20151015	57310	$i_{P1}r_{P1}z_{P1}y_{P1}$	30,60,200	72
20151017	57312	i_{P1}	60	5
20151018	57313	$i_{P1}r_{P1}z_{P1}y_{P1}$	30,80,200	70
20151019	57314	$i_{P1}r_{P1}z_{P1}y_{P1}$	35,200	22
20151021	57316	$i_{P1}r_{P1}z_{P1}y_{P1}$	30,45,50,200	98
20151022	57317	$i_{P1}r_{P1}z_{P1}y_{P1}$	30,45,60,200	79
20151023	57318	$i_{P1}r_{P1}z_{P1}y_{P1}$	30,60,65,200	87
20151024	57319	$i_{P1}r_{P1}z_{P1}y_{P1}$	30,45,200	102
20151025	57320	$i_{P1}r_{P1}z_{P1}y_{P1}$	30,60,65,200	90
20151026	57321	$i_{P1}r_{P1}z_{P1}$	35,50,60,200	64

Table A2. Proximity to twilight of Pan-STARRS1 fields

Date	Plot	LST of twilight			RA of an HA = 4.5 hrs at twilight		
		16 deg i_{P1} -band	14 deg z_{P1} -band	10 deg y_{P1} -band	i_{P1} -band	z_{P1} -band	y_{P1} -band
17 Sept	first 3 days	04:27	04:36	04:53	08:57 134.25	09:06 136.50	09:23 140.75
27 Sept	3-10 days	05:09	05:18	05:35	09:39 144.75	09:48 147.00	10:05 151.25
4 Oct	10-17 days	05:39	05:47	06:05	10:09 152.25	10:17 154.25	10:35 158.75
11 Oct	17-24 days	06:08	06:17	06:34	10:38 159.50	10:47 161.75	11:04 166.00
18 Oct	24-31 days	06:38	06:47	07:04	11:08 167.0	11:17 169.25	11:34 173.50
25 Oct	> 31 days	07:08	07:17	07:34	11:38 174.5	11:47 176.75	12:04 181.00